Fluid Mechanics of Planktonic Microorganisms

Jeffrey S. Guasto,[1,2] Roberto Rusconi,[1] and Roman Stocker[1]

[1]Department of Civil and Environmental Engineering, Massachusetts Institute of Technology, Cambridge, Massachusetts 02139; email: jguasto@mit.edu, rrusconi@mit.edu, romans@mit.edu

[2]Department of Ecology and Evolutionary Biology, University of California, Los Angeles, California 90095

Annu. Rev. Fluid Mech. 2012. 44:373–400

First published online as a Review in Advance on October 10, 2011

The *Annual Review of Fluid Mechanics* is online at fluid.annualreviews.org

This article's doi: 10.1146/annurev-fluid-120710-101156

0066-4189/12/0115-0373$20.00

Keywords

swimming, low–Reynolds number flow, shear, transport, nutrient uptake

Abstract

The diversity of the morphologies, propulsion mechanisms, flow environments, and behaviors of planktonic microorganisms has long provided inspiration for fluid physicists, with further intrigue provided by the counterintuitive hydrodynamics of their viscous world. Motivation for studying the fluid dynamics of microplankton abounds, as microorganisms support the food web and control the biogeochemistry of most aquatic environments, particularly the oceans. In this review, we discuss the fluid physics governing the locomotion and feeding of individual planktonic microorganisms ($\leq$1 mm). In the past few years, the field has witnessed an increasing number of exciting discoveries, from the visualization of the flow field around individual swimmers to linkages between microhydrodynamic processes and ecosystem dynamics. In other areas, chiefly the ability of microorganisms to take up nutrients and sense hydromechanical signals, our understanding will benefit from reinvigorated interest, and ample opportunities for breakthroughs exist. When it comes to the fluid mechanics of living organisms, there is plenty of room at the bottom.

1. PLANKTON IN MOTION: ECOLOGICAL CONSIDERATIONS

Phytoplankton: photosynthetic plankton that produce oxygen and biomass and form the base of aquatic food webs; some are motile

Heterotrophic bacteria: unicellular prokaryotic microorganisms that take up organic carbon as an energy source, whereas some other bacteria use light (e.g., cyanobacteria)

Fluid mechanics governs a wide range of functions for planktonic organisms, from propulsion to nutrient uptake to fertilization. Etymologically, *planktos* ($\pi\lambda\alpha\gamma\kappa\tau o\sigma$), from Greek, means wanderer or drifter. Plankton include a broad spectrum of organisms, from bacteria to jellyfish. Here we consider microbial plankton (~0.1–1,000 μm), which live mostly at low Reynolds number, and describe how they swim, how they are affected by ambient flow, and how they feed.

Microorganisms are among the most important life-forms on Earth, not only because of their diversity and cumulative biomass, but also because of their functions in ecosystems. Oceans provide the largest reservoirs of planktonic microorganisms. Phytoplankton form the base of the marine food web and produce nearly half of the world's oxygen (Field et al. 1998). Heterotrophic bacteria—whose role remained underappreciated (Pomeroy 1974) until the introduction of the concept of a microbial loop (Azam et al. 1983)—are the recyclers of dissolved organic matter and fuel a sizable fraction of the oceans' biogeochemical cycles, such as the carbon cycle, by transferring dissolved resources to larger organisms (Kirchman 2008). All their predators, and subsequent trophic levels up to millimeter-sized copepods (**Figure 1*e***), live at low Reynolds numbers. Flow mediates many processes crucial to the ecology of the microbial food web, including motility, nutrient uptake, and cell-cell encounters. Yet fast-paced discoveries on the diversity, metabolic functions, behaviors, and spatial distribution of microbes in the sea (Johnson et al. 2006, Moran et al. 2004, Seymour et al. 2010) are rarely interpreted in the context of flow and transport.

A fundamental determinant of microbial life is morphology (Dusenbery 2009, Young 2006). Most bacteria are round or moderately elongated, generally ranging in size from 0.3 to 3 μm (although some measure nearly 1 mm) (**Figure 1*j*,*m*,*n***). Phytoplankton, <1 μm to a few millimeters in size, are morphologically much more diverse and can live as single cells (**Figure 1*a*,*c*,*d*,*g*,*h***) or colonies (**Figure 1*b***), often arranged in chains (**Figure 1*f***). Their beauty and morphological complexity (**Figure 1**) have amazed generations of ecologists (Naselli-Flores et al. 2007), but the adaptive significance of their form often remains unknown.

Size affects metabolism, as small cells with their large surface-to-volume ratios are better equipped to take up dissolved nutrients by osmosis (Kiørboe 2008). Size also affects motility,

Figure 1

Mosaic showing the complexity and diversity of planktonic microorganisms. Scale bars are approximate. (*a*) Scanning-electron-microscopy (SEM) image of the widespread coccolithophore *Emiliania huxleyi*, whose armored appearance is due to calcium-carbonate platelets (coccoliths). Figure courtesy of Jeremy Young, Natural History Museum, London. (*b*) Dark-field image of the colonial green alga *Volvox carteri*. Figure courtesy of Knut Drescher, Princeton University. (*c*) SEM image of the marine diatom *Thalassiosira pseudonana*. The cell wall of diatoms, called a frustule, is made of silica and is of great interest for nanotechnology (Kröger & Poulsen 2008). Figure courtesy of Nils Kröger, Georgia Institute of Technology. (*d*) The biflagellate green alga *Chlamydomonas reinhardtii*. Figure reproduced from Drescher et al. (2009) with permission. (*e*) The copepod *Pareuchaeta norvegica*. Note the mechanosensory setae on the antennae. Figure courtesy of Erik Selander, Technical University of Denmark. (*f*) A chain of the diatom *Thalassiosira* sp. Figure courtesy of David Townsend, University of Maine. (*g*) SEM image of the dinoflagellate *Ornithocercus thumii*. Figure courtesy of Maria Faust and the Department of Botany, Smithsonian Institution. (*h*) The dinoflagellate *Ceratium ranipes*, which produces so-called fingers by day, only to adsorb them at night. Figure reproduced from Pizay et al. (2009) with permission. (*i*) SEM image of the ciliate *Paramecium caudatum*. Figure courtesy of Wilhelm Foissner and Andreas Zankl, University of Salzburg. (*j*) Immobilized, fluorescently labeled *Escherichia coli* bacterium. Figure reproduced from Turner et al. (2000) with permission. (*k*) SEM image of sea-urchin spermatozoa attempting to fertilize an egg. Figure courtesy of David Epel, Stanford University. (*l*) A natural assemblage of phytoplankton from the Gulf of Maine, including *Stephanopyxis* sp., *Thalassionema* sp., *Eucampia* sp., and *Chaetoceros* sp. Figure courtesy of David Townsend, University of Maine. (*m*) Electron micrograph of the bacterium *Vibrio parahaemolyticus*. Figure reproduced from McCarter et al. (1988) with permission. (*n*) SEM image of the marine cyanobacteria *Prochlorococcus*, one of the most-abundant photosynthetic organisms on Earth (Chisholm et al. 1988). *Prochlorococcus* is nearly spherical and nonmotile. Figure courtesy of Anne Thompson, Massachusetts Institute of Technology.

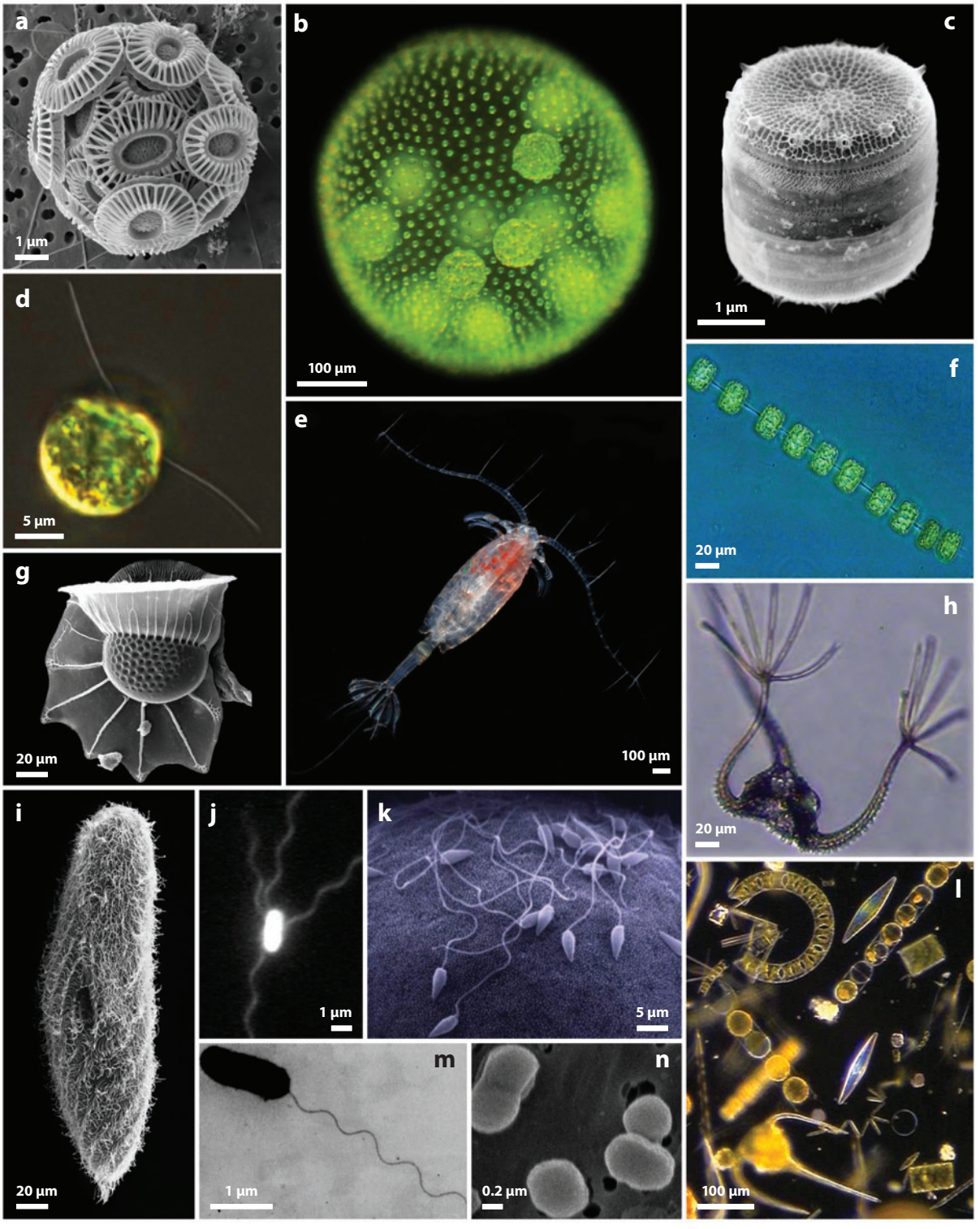

which competes with random Brownian motion and is predicted to be of use when plankton are larger than ≈0.6 μm in diameter (Dusenbery 2009), in line with the observation that the smallest bacteria are not motile. Another important morphological parameter is elongation. Small plankton (1–2 μm) tend to be spherical, and elongation on average increases with size (Jonasz 1987). Most phytoplankton species are nonspherical, with a mean aspect ratio of ≈5 (Clavano et al. 2007), and only ≈20% of bacterial genera are spherical, the rest having on average an aspect ratio of ≈3 (Dusenbery 2009). Motile bacteria tend to be more elongated than nonmotile ones, possibly to optimize swimming and the detection of chemical gradients (Dusenbery 2009).

Microorganisms have several traits that distinguish them from passive particles. The most dramatic is motility, which allows them to move relative to the ambient flow to seek food or escape predators. Planktonic microorganisms swim by means of flagella, which come in two varieties, prokaryotic and eukaryotic. The prokaryotic flagellum comprises a basal body, a hook, and a filament (Namba & Vonderviszt 1997). The basal body anchors the flagellum in the cell membrane and contains a rotary proton or sodium motor, rotating at 100–1,000 Hz. Outside the cell wall, the hook connects the motor to the filament, which is ≈10 μm long and ≈20 nm in diameter and is made of the protein flagellin (Berg 2004). Flagellin gives the flagellum a helical shape, with a pitch of 2–3 μm and a diameter of ≈0.4 μm (**Figure 1*j*,*m***), which is essential for locomotion.

The eukaryotic flagellum, found in dinoflagellates (**Figure 1*g*,*b***) and spermatozoa (**Figure 1*k***), is markedly different. At its core is the axoneme, which propagates bending waves down the flagellum (Rikmenspoel 1978) at a frequency of 10–60 Hz in the case of sperm, for example. The axoneme, 200–400 nm in diameter and 10–100 μm long, comprises microtubule doublets having a 9 + 2 configuration, in which nine microtubule doublets surround two central, single microtubules. Dynein arms on the outer doublets, powered by ATP, generate internal shear by sliding along tubules, thus actuating the flagellum along its entire length (Brennen & Winet 1977).

Having been among the first low–Reynolds number swimmers to be studied in detail, sperm cells have played an important role in understanding swimming in viscous fluids and flagellar mechanics (Gray & Hancock 1955, Hancock 1953, Machin 1958). The head of the sperm cell, which carries the genetic material, is typically ≈5 μm in size, whereas the flagellum is often 30–80 μm long (Brennen & Winet 1977). Exceptions abound, however, including the needle-like heads of avian spermatozoa and the double-helical flagella of insect sperm cells (Brennen & Winet 1977). The planar or helical flagellar waves (Ishijima et al. 1992, Woolley & Vernon 2001) can propel a sperm cell at several hundred micrometers per second (Böhmer et al. 2005) and often result in helical swimming trajectories. In contrast to prokaryotes, spermatozoa can actively turn to maneuver within gradients of chemoattractants released by an egg (Böhmer et al. 2005).

Other eukaryotes, such as *Chlamydomonas* (**Figure 1*d***) and *Dunaliella*, swim by beating two anterior flagella at ≈50 Hz in a breaststroke motion. During the power stroke the flagella sweep backward, remaining mostly perpendicular to the swimming direction to maximize thrust. This pulls the cell forward (Rüffer & Nultsch 1985). Ciliates, including the unicellular *Paramecium* (**Figure 1*i***) and the colonial alga *Volvox* (**Figure 1*b***), use thousands of cilia for locomotion (Brennen & Winet 1977). Cilia have the same internal structure but are typically shorter than flagella and beat at 5–30 Hz in a planar or helical fashion (Brennen & Winet 1977, Childress 1981).

A second trait that distinguishes microorganisms from passive particles is the ability to control settling rates, achieved by regulating form resistance or buoyancy. The spines of many diatoms (Walsby & Xypolyta 1977) and dinoflagellates (Zirbel et al. 2000) decrease settling rates by increasing drag (Padisák et al. 2003), whereas gas vesicles (Walsby 1994), carbohydrate ballasting (Villareal & Carpenter 2003), and ion replacement (Boyd & Gradmann 2002, Sartoris et al. 2010) are mechanisms for buoyancy control. Stokes's law predicts an increase of settling speed with the

Dinoflagellates: large group of flagellated eukaryotic microorganisms, with about half being photosynthetic; often dominant in weakly turbulent, stratified waters with low surface nutrient concentrations

Prokaryotes: organisms lacking a cell nucleus; comprise bacteria and archaea

Eukaryotes: organisms having a cell nucleus

Diatoms: major group of photosynthetic eukaryotic microorganisms, often dominant in turbulent, nutrient-rich conditions; are nonmotile and encased in a silica shell called a frustule

square of length, R. The weaker dependence of speed on radius ($\sim R^{1.2-1.6}$) actually exhibited by diatoms (**Figure 1*c***) has long puzzled oceanographers, and it was recently found to result from a decrease in diatom density with increasing size (Miklasz & Denny 2010).

The third trait is sensing, which is used by microorganisms to detect physical or chemical gradients and bias their motility accordingly (taxis). Many directional responses are known, from chemotaxis (Berg 2004) to aerotaxis (Taylor et al. 1999), thermotaxis (Paster & Ryu 2008), magnetotaxis (Frankel et al. 1997), and phototaxis (Engelmann 1883). Chemotaxis is the most widely studied of these directional movements, and the bacterium *Escherichia coli* (**Figure 1*j***) has long served as the chemotactic model organism of choice (Berg 2004), yet marine bacteria display specific motility and chemotaxis adaptations that we briefly discuss below.

A fourth trait is feeding, for example, through the uptake of dissolved nutrients (e.g., nitrate, phosphate, iron), which is paramount for most microorganisms. External or self-generated flow can increase nutrient transport and uptake. Although many microscale swimmers must optimize uptake simultaneously with propulsion, to date much more attention has been devoted to the latter (Lauga & Powers 2009).

The sheer diversity of organisms makes the task of reviewing microbial fluid mechanics daunting. We focus on planktonic microorganisms and, with regard to foraging, on those that feed on dissolved nutrients. We thus do not include surface-attached microbes or filter feeders (which forage on particles). We also do not address dense aggregations, such as swarms, which have recently been reviewed (Koch & Subramanian 2011) and are uncommon in the bulk of oceans and lakes, to which we primarily refer.

2. THE MICROHYDRODYNAMICS OF SWIMMING PLANKTON

Most planktonic microorganisms live in a world dominated by viscous forces, governed by physical rules that are far different from those of macroorganisms and that are sometimes counterintuitive. In this section, we discuss the general properties of viscous flows and their implications for swimming microorganisms. Our aim is not to present a mathematically comprehensive treatment, which can be found elsewhere (Brennen & Winet 1977, Lauga & Powers 2009, Leal 2007, Lighthill 1976), but to provide a physical overview sufficient to appreciate the fluid mechanics of planktonic microorganisms.

2.1. Low–Reynolds Number Swimming

For planktonic microorganisms, water is an incompressible Newtonian liquid, although dense suspensions can be non-Newtonian (Jenkinson 1986). The Navier-Stokes equation, made dimensionless by appropriate length, time, and velocity scales (L, T, and U, respectively),

$$\frac{\mathrm{Re}}{\mathrm{Sr}}\frac{\partial \tilde{\mathbf{u}}}{\partial \tilde{t}} + \mathrm{Re}\,\tilde{\mathbf{u}}\cdot\tilde{\nabla}\tilde{\mathbf{u}} = \tilde{\nabla}^2\tilde{\mathbf{u}} - \tilde{\nabla}\tilde{p} + \tilde{\mathbf{f}}, \tag{1}$$

together with the continuity condition ($\tilde{\nabla}\cdot\tilde{\mathbf{u}} = \mathbf{0}$) specifies the fluid motion, where $\tilde{\mathbf{u}} = \mathbf{u}/U$ is the fluid velocity, $\tilde{p} = pL/\mu U$ is the pressure, $\tilde{\mathbf{f}} = \mathbf{f}\,L^2/\mu U$ is an external body force, and tildes denote nondimensional variables (Leal 2007). The Reynolds number, $\mathrm{Re} = \rho UL/\mu$, where ρ and μ are the fluid density and viscosity, respectively, measures the relative magnitude of inertial and viscous forces, whereas the Strouhal number, $\mathrm{Sr} = TU/L$, compares a forcing timescale to the flow timescale. Microorganisms live at low Reynolds numbers ($\mathrm{Re} \ll 1$), in which fluid motion is dominated by viscous forces, and the Navier-Stokes equation reduces to the Stokes equation

$$\nabla p = \mu\nabla^2\mathbf{u} + \mathbf{f}, \tag{2}$$

provided also that $\mathrm{Re}/\mathrm{Sr} \ll 1$. For example, an $L = 10$-μm-radius flagellate swimming at $U = 100\ \mu\mathrm{m\ s}^{-1}$ with a flagellar beat period $T = 1/100$ s has $\mathrm{Re} = 10^{-3}$, $\mathrm{Sr} = 10^{-1}$, and $\mathrm{Re}/\mathrm{Sr} = 10^{-2}$. Under the effect of its own drag, the flagellate would come to rest within 10 nm if it were to suddenly stop beating its flagellum, demonstrating the negligible role of inertia.

The Stokes equation has several important properties (Leal 2007) that affect microbial locomotion (Purcell 1977). First, it is pseudosteady: The absence of a time derivative implies that temporal changes enter only via moving boundary conditions, such as flagella, to which the flow responds instantaneously. As a consequence, the net motion of a swimmer is independent of the rate at which its body deforms. Second, the Stokes equation is linear; hence the solution of the flow fields around complex structures can be assembled by superposition. Third, linearity, together with pseudosteadiness, implies reversibility: A reversal of the boundary conditions results in a change of sign in the velocity and pressure fields. For example, the drag on a rigid body is the same upon flow reversal. For sustained swimming, a body must deform in a time-periodic fashion, but linearity and reversibility forbid reciprocal motions, those which appear the same when viewed forward and backward in time, from generating any propulsion. This is Purcell's (1977) scallop theorem, so named because it predicts that a device with one degree of freedom (e.g., two rigid flaps connected by a hinge) cannot swim at low Reynolds numbers. Examples of successful biological propulsion systems, which bypass the constraints of the scallop theorem, are the rotation of a rigid helical filament by prokaryotes and the nonreciprocal motion of deformable flagella by which eukaryotes swim (Gray & Hancock 1955, Rüffer & Nultsch 1985).

2.2. Flagellar Hydrodynamics

Microorganisms swim using drag-based thrust, taking advantage of the drag anisotropy of their slender appendages, whereby the drag coefficient $\xi_\perp$ normal to a filament section is larger than that in the parallel direction, $\xi_\parallel$ (Brennen & Winet 1977, Childress 1981, Lauga & Powers 2009). By waving or rotating their flagella so that they are mostly perpendicular to the direction of travel, flagellates escape the perils of reversibility and produce thrust. Taylor (1951) first considered propulsion due to traveling waves along flagella, and shortly thereafter, Gray and Hancock (Gray & Hancock 1955, Hancock 1953) developed resistive-force theory to describe the forces on a sperm flagellum. In resistive-force theory, drag is assumed to act only locally, with resistance coefficients (per unit length) given by $\xi_\parallel = 2\pi\mu/(\ln 2\frac{L}{a} - \frac{1}{2})$ and $1.5 \leq \xi_\perp/\xi_\parallel \leq 2$, where a is the filament radius and L its typical wavelength (Childress 1981, Lighthill 1976). This theory, often used because it is physically intuitive, has been successfully applied to predict forces on flagella and trajectories of spermatozoa (Johnson & Brokaw 1979). However, hydrodynamic interactions between different parts of the organism can degrade the accuracy of resistive-force-theory predictions. Whereas hydrodynamic interactions between the body and flagellum have a minimal impact, nonlocal interactions within the flagellum can be important (Chattopadhyay & Wu 2009). For example, in one case resistive-force theory was found to overestimate swimming speeds in *E. coli* by up to a factor of two when compared with experiments (Chattopadhyay & Wu 2009). This was confirmed using the more accurate (and computationally intensive) approach of slender-body theory, which accounts for nonlocal effects and arbitrary filament shapes through a distribution of singularities, leading to an integral relation for the forces on the flagellum (Johnson & Brokaw 1979, Wu 1977).

The elasticity of eukaryotic flagella implies that waveforms are affected by external stresses. The observed waveforms emerge from the competition between elastic forces, internal shear due to filament sliding (Mitchison & Mitchison 2010), and external viscous stresses (Gadêlha et al. 2010, Gaffney et al. 2011). The sperm number, $\mathrm{Sp} = L(\omega\xi_\perp/G)^{1/4}$, measures the relative importance of viscous and elastic stresses, where L is the flagellum length, ω its beat frequency, and G its

bending modulus (Gadêlha et al. 2010, Lauga & Powers 2009). For Sp $\ll$ 1, internal stresses dominate and determine the flagellar waveform, whereas for Sp > 1, viscous stresses can alter beat frequencies and wavelengths (Woolley & Vernon 2001) and trigger elasto-hydrodynamic instabilities (Gadêlha et al. 2010).

Viscous stresses transmitted through the ambient fluid are also thought to be responsible for the synchronization of flagella and cilia (Goldstein et al. 2009, Machin 1963). Recently it was shown that periods of noisy synchronization and phase lags between *Chlamydomonas* flagella are consistent with hydrodynamic interactions (Goldstein et al. 2009). Every ∼10 s, changes in the relative phase of the beating flagella (phase slips) lead to sharp turns, which interrupt periods of mostly straight swimming in a eukaryotic version of run-and-tumble motility (Polin et al. 2009).

Run-and-tumble: motility pattern of peritrichous bacteria, which alternate straight swimming with nearly random reorientations, resulting in a random walk

Cilia, in *Paramecium*, for example (**Figure 1*i***), also execute coordinated motions with a high degree of organization, called metachronal waves (Guirao & Joanny 2007), which result from the coupling of axoneme dynamics through hydrodynamic interactions (Gueron et al. 1997). These ≈10–40-μm-long waves (Brennen & Winet 1977, Childress 1981) travel at >100 μm s^{-1} and might reduce the energetic cost of locomotion (Gueron & Levit-Gurevich 1999, Michelin & Lauga 2010). Similar to *Paramecium*, the coordinated flagella on *Volvox* beat mostly from one pole to the other, with a slight twist that causes the organism to rotate. When cells sense directional illumination from the side, flagellar beating is locally downregulated for phototaxis. The relative timing of the flagellar beat recovery and the angular velocity of the organism were shown to be crucial for the cilia to act in concert and enable *Volvox* to execute turns during phototaxis (Drescher et al. 2010b).

2.3. Propulsion Cost and Efficiency

Propulsion efficiency at low Reynolds numbers is notoriously low (∼1%–3%), fundamentally because thrust is generated by the same mechanism that resists motion: viscous drag. Current belief holds that microbial swimming incurs a small metabolic cost, based on Purcell's (1977) calculation for *E. coli*, which swims slowly (15–30 μm s^{-1}) in a nutrient-rich environment. It has been suggested that this conclusion does not apply to fast swimmers (∼100 μm s^{-1}) in oligotrophic (i.e., nutrient-poor) environments (Mitchell et al. 1996), including many marine microorganisms, for which speed is limited by cost (Taylor & Stocker 2011).

This low efficiency notwithstanding, many flagellar morphologies and beat patterns appear to be optimized for locomotion (Spagnolie & Lauga 2011, Tam & Hosoi 2011a). The mechanical or Froude efficiency, $\mathcal{E} = \xi_0 \langle U \rangle^2 / \langle \mathcal{P} \rangle$, is the ratio of the power required to tow a body, having a drag coefficient ξ_0, at its beat-cycle averaged speed $\langle U \rangle$, to the beat-cycle averaged power $\langle \mathcal{P} \rangle$ exerted by the swimmer on the fluid (Lighthill 1952). $\langle \mathcal{P} \rangle$ can be computed from the viscous dissipation in the surrounding fluid (Childress 1981), as $\mathcal{P} = 2\mu \int_{\mathcal{V}} \mathbf{E} : \mathbf{E}\, d\mathcal{V}$, where $\mathbf{E} = \frac{1}{2}[\nabla \mathbf{u} + \nabla \mathbf{u}^T]$ is the rate of strain tensor (Leal 2007). Because the typical goal of a swimmer is to transport a payload (i.e., the body), this definition of efficiency differs from that of a swimming sheet or headless flagellum, in which the numerator is the power to tow a filament in its straightened configuration (Childress 1981).

Whereas the optimization of sperm swimming has been considered using analytically tractable approximations (including resistive-force theory) with traveling waves and headless swimmers (Lighthill 1976, Pironneau & Katz 1974), a more general approach based on slender-body theory has been recently proposed (Tam & Hosoi 2011b). This optimization predicts a flagellum-to-head length ratio of ≈12 for maximum efficiency, in good agreement with the sperm morphology of many mammal species (Tam & Hosoi 2011b). When similar optimization techniques were applied to the beat patterns of biflagellates, commonly observed waveforms emerged as local maxima of mechanical efficiency, including the breaststroke ($\mathcal{E}$ = 0.8%) and the undulatory

stroke ($\mathcal{E} = 0.14\%$) (Tam & Hosoi 2011a). For bacteria, it has been shown that the most common polymorphic state of the flagellum, the normal form (see Section 3.3), is the one that maximizes propulsion efficiency (Spagnolie & Lauga 2011). Experiments on this topic are few but include elegant optical-trap measurements (Chattopadhyay et al. 2006), which yielded $\mathcal{E} \approx 2\%$ for *E. coli*, in good agreement with predictions (1%–3%) (Purcell 1977, Spagnolie & Lauga 2011).

With their short appendages ($\leq$10 μm) beating close to the body, ciliates might be expected to be inefficient. Yet their efficiency is comparable with that of uniflagellates (Childress 1981) because of cooperative effects among cilia (Gueron & Levit-Gurevich 1999). Estimates of stroke efficiency in ciliates are often limited to the assumption of traveling-wave solutions and/or small-amplitude deformations of the ciliary envelope (Lighthill 1952, Blake 1971, Stone & Samuel 1996). By allowing unconstrained surface deformations and requiring only time-periodic solutions, one can see that traveling surface waves on squirmers, reminiscent of metachronal waves, emerge naturally as the optimal propulsion kinematics (Michelin & Lauga 2010). Efficiency further depends on the arrangement of the cilia. Simulations show that the equatorial ciliary belt of the red-tide forming ciliate *Mesodinium rubrum* allows it to achieve a fivefold larger efficiency than if the belt were located near one of the poles (Jiang 2011).

Pushers: microorganisms having locomotory appendages behind the cell body, relative to the swimming direction

Pullers: microorganisms having locomotory appendages in front of the cell body, relative to the swimming direction

2.4. Swimming as a Singularity

A fundamental building block of many solutions to the Stokes equation is the flow field due to a point force, $\mathbf{f} = \delta(\mathbf{x})\hat{\mathbf{f}}$ (where $\hat{\mathbf{f}}$ is the force vector), known as the Stokeslet (Hancock 1953):

$$\mathbf{u}_S(\mathbf{x}) = \frac{\hat{\mathbf{f}}}{8\pi\mu} \cdot \left[\frac{\mathbf{I}}{r} + \frac{\mathbf{xx}}{r^3}\right]. \tag{3}$$

In the absence of external forces, self-propelled swimmers exert no net force or torque on the fluid: Thrust is balanced by drag (Lauga & Powers 2009). For example, the flagellum pushes a bacterium forward with a thrust $\hat{\mathbf{f}}$, and the body experiences a drag $-\hat{\mathbf{f}}$. The small separation $\mathbf{b}$ between the centers of drag and thrust suggests that the flow generated by the cell behaves as a force dipole $\mathbf{u}_{SD}$, comprising two opposing Stokeslets. The symmetric part of the force dipole, corresponding to colinear, opposing Stokeslets, is the stresslet (Leal 2007):

$$\mathbf{u}_{SS} = \frac{1}{8\pi\mu}\left[\frac{\hat{\mathbf{f}}\cdot\mathbf{b}}{r^3} + 3\frac{(\hat{\mathbf{f}}\cdot\mathbf{x})(\mathbf{b}\cdot\mathbf{x})}{r^5}\right]\mathbf{x}. \tag{4}$$

Because derivatives of the Stokeslet are also solutions of the Stokes equation, a formal multipole expansion of the point-force solution (Equation 3) leads to a set of fundamental singularity solutions including the force dipole, force quadrupole, and higher-order terms (Leal 2007). Linear combinations of them, in addition to the source dipole term [a singularity solution consisting of a mass source and mass sink separated by a small distance (Lauga & Powers 2009)], can be used to describe the flow of a general swimmer.

This classic prediction for pushers, often used in models, has only recently been verified experimentally using particle tracking to measure the flow field around free-swimming, 2-μm-long bacteria (Drescher et al. 2011). The measured velocity field in the vicinity of *E. coli* (**Figure 1*j***) has the classic characteristics of a stresslet, with a slight anterior-posterior asymmetry due to the presence of the long flagellum (**Figure 2*a***).

Biflagellate pullers have similarly been described by a stresslet, but one of opposite sign, as their locomotory apparatus is in front. Whereas observations of *Chlamydomonas reinhardtii* (**Figure 1*d***) show the typical r^{-2} velocity scaling of a stresslet with distance (Drescher et al. 2010a), the flow field averaged over a beat cycle departs strongly from a stresslet, exhibiting a hyperbolic stagnation point

SWIMMING NEAR BOUNDARIES

Nearby boundaries can have striking effects on swimming. It has long been observed that pushers, such as bacteria and spermatozoa, are attracted to solid surfaces (Rothschild 1963). This effect can be rationalized by considering the flow field induced by the stresslet associated with a pusher swimming parallel to a no-slip wall, which draws in fluid from its sides and pushes fluid away anteriorly and posteriorly (Lauga & Powers 2009). The swimmer and its image singularity exert an attractive force, pulling one another toward the wall (Lauga & Powers 2009). In addition to hydrodynamic forces, oblique collisions between swimmers and solid boundaries cause the cells to reorient and swim parallel to the wall, further enhancing the trapping effect, as few mechanisms are available to eject pushers from surfaces (e.g., Brownian rotation and tumbling) (Drescher et al. 2011, Li & Tang 2009). The counter-rotation of the cell body and flagella, combined with their differential hydrodynamic traction near the solid boundary, causes cells to swim in circles (DiLuzio et al. 2005). Analogously, cells swim in circles of the opposite orientation underneath an air-water (perfect-slip) interface (Di Leonardo et al. 2011).

≈6 radii in front of the organism and strong lateral vortices (**Figure 2*b***). A simple model based on singularity solutions still captures the flow field accurately, but three rather than two Stokeslets are required: one representing the body and two, of opposite direction and half-strength, representing the flagella. Furthermore, time-resolved measurements for cells swimming in a thin liquid film showed that the flow field of *C. reinhardtii* is highly unsteady and evolves dramatically throughout the beat cycle, which takes just 20 ms (**Figure 2*c***) (Guasto et al. 2010). This unsteadiness results in a fourfold increase in power expenditure compared with steady swimming (Guasto et al. 2010).

Not all swimmers are force-free, and a small contribution from buoyancy can severely modify a microorganism's flow field. Drescher et al. (2010a) measured the flow around *Volvox carteri* (**Figure 1*b***), a spherical green alga composed of a 200–600-μm shell of thousands of *Chlamydomonas*-like cells beating their flagella, and fit multipoles to the observations. Unexpectedly, they found the dominant term to be the Stokeslet (**Figure 2*d***), which results from *V. carteri*'s slight negative buoyancy (making it non-force-free), followed by the source dipole, which comes from the no-slip condition at the cell surface (**Figure 2*e***). The latter finding is analogous to the case of *Paramecium*, whose flow field is also closer to a source doublet than a force dipole (Keller & Wu 1977).

Density stratification, generated by temperature or salinity gradients, can dramatically change a swimmer's flow field, by partially confining vertical fluid motion. For weak density gradients, Ardekani & Stocker (2010) found that stratification affects organisms as small as $O(100\ \mu m)$ and causes Stokeslet and stresslet flow fields (stratlets) to roll up in toroidal vortices. This increases the decay rate of fluid velocity with distance from the organism, rendering swimmers stealthier than in homogeneous fluids.

Some microorganisms exhibit impressive jumps that propel them out of the low–Reynolds number world. *M. rubrum* achieves $\mathrm{Re} \sim 1$ (Jiang 2011) to enhance nutrient uptake, and ambush-feeding copepods (**Figure 1*e***) reach $\mathrm{Re} \sim 30$–100 by jumping at $\sim 100\ \mathrm{mm\ s^{-1}}$ to minimize their boundary layer for stealthy prey attacks (Kiørboe et al. 2009). The copepod kicks the water with its swimming legs, generating two counter-rotating, viscous vortex rings that have been described using the impulsive stresslet, despite the intermediate Reynolds number (Jiang & Kiørboe 2011b), a singularity solution of the unsteady Stokes equation consisting of two equal and opposite impulsive momentum sources acting a small distance apart (Afanasyev 2004). The flow field decays like r^{-4} in the far field, making this a stealthy propulsion mechanism if sufficiently impulsive. Impulsiveness can be quantified by the jump number, $N_{jump} = \tau(4\nu)/L^2$, measuring the power

stroke duration τ relative to the viscous timescale $L^2/(4\nu)$, where L is the length of the beating appendage. N_{jump} corresponds to four times the parameter $(\mathrm{Re/Sr})^{-1}$, which scales the unsteady acceleration in Equation 1. Vortex rings are generated for $N_{jump} < 1$, setting a lower size threshold (~50–200 μm) for stealthy jumps. The ability to break the low–Reynolds number barrier affords organisms a marked increase in efficiency, with *M. rubrum* achieving $\mathcal{E} \approx 78\%$ (Jiang 2011) and copepods reaching $\mathcal{E} \geq 94\%$ (Jiang & Kiørboe 2011a).

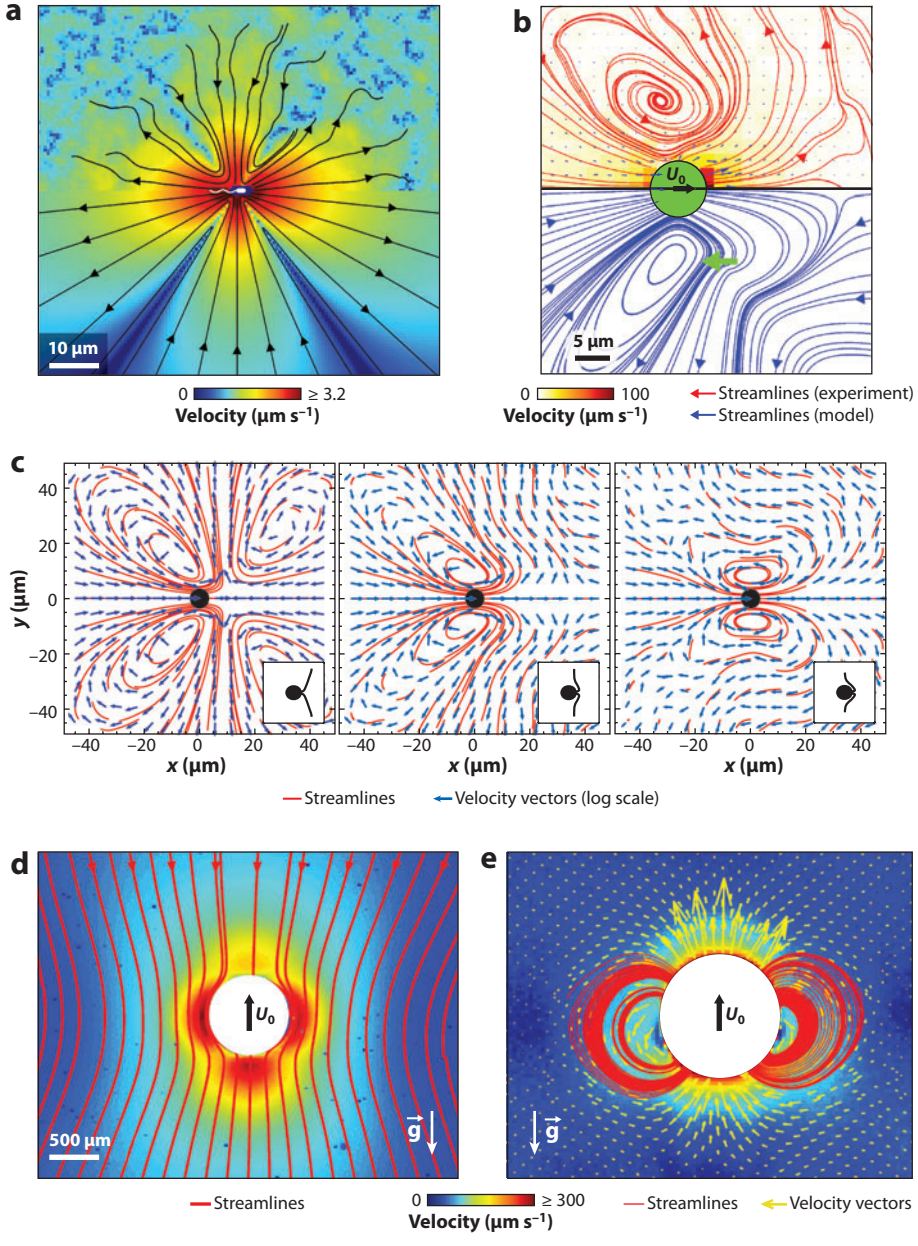

3. LOCOMOTION IN FLOW

3.1. Elongation

Jeffery orbits: periodic rotational trajectories of elongated particles or microorganisms in shear, in which the angular speed varies with orientation relative to the flow

Even in the absence of motility, morphology can dramatically affect the function of plankton in flow (**Figure 3*a*,*b***). For example, elongation modifies flow-induced cell rotation (**Figure 3*a***), affecting nutrient uptake (see Section 4.2) and entrainment in copepod feeding currents (Visser & Jonsson 2000). For $\mathrm{Re} = 0$, the centroid of an elongated particle follows the streamline of the underlying flow, while the body undergoes periodic Jeffery orbits (Jeffery 1922). During a Jeffery orbit, the ends of the major axis describe a spherical ellipse in a coordinate frame moving with the centroid. Highly elongated particles spend most of their time aligned with streamlines, flipping orientation with a period $T = 2\pi\dot{\gamma}^{-1}(q + q^{-1})$ that increases with aspect ratio q, decreases with shear rate $\dot{\gamma}$, and applies to most bodies of revolution (Bretherton 1962). The unit vector $\mathbf{p}$ of cell orientation obeys

$$\dot{\mathbf{p}} = \frac{1}{2}\,\boldsymbol{\omega} \times \mathbf{p} + \beta \mathbf{p} \cdot \mathbf{E} \cdot (\mathbf{I} - \mathbf{pp}), \tag{5}$$

where $\boldsymbol{\omega}$ is the vorticity vector, and $\beta = (q^2 - 1)/(q^2 + 1)$ for ellipsoids of revolution (Bretherton 1962, Pedley & Kessler 1992). Rotational Brownian motion destroys the preferential alignment induced by shear when the Péclet number, $\mathrm{Pe}_r = \dot{\gamma}/D_r$ (where D_r is the rotational diffusivity), is smaller than 1.

Jeffery's predictions have been verified for passive inert particles (Trevelyan & Mason 1951), whereas plankton have received little attention despite their prevalent elongation (**Figure 3*a***). High-speed imaging of nonflagellated *E. coli* in a microfluidic shear flow has revealed Jeffery

Figure 2

Flow fields around individual self-propelled microorganisms. The flows generated by swimming microorganisms are often approximated by a superposition of singularities, such as Stokeslets, stresslets, and source dipoles. Only recently have these theories been tested for pushers, pullers, and ciliates, due largely to experimental advances in microscale particle tracking. (*a*) The measured velocity field (*upper half*) in the vicinity of the pusher bacterium *Escherichia coli* (2-μm-long body) has the classic characteristics of a stresslet (*lower half*; theoretical fit to data) with a slight anterior-posterior asymmetry due to the long flagellum. Figure modified from Drescher et al. (2011) with permission. (*b*) The flow fields of other swimmers, such as the 10-μm-diameter biflagellated puller *Chlamydomonas reinhardtii*, are far from the predicted stresslet, exhibiting a hyperbolic stagnation point and a toroidal vortex when averaged over the flagellar beat cycle (*upper half*). A model consisting of three Stokeslets—one representing the body (*black arrow*) and two, of opposite direction and half-strength, representing one flagellum each (*green arrow*)—captures the main features of the flow (*lower half*). Figure modified from Drescher et al. (2010a) with permission. Copyright 2010 by The American Physical Society. (*c*) The flow field generated by *C. reinhardtii* is highly unsteady and evolves dramatically throughout the beat cycle, which takes just 20 ms. This is demonstrated by the time-resolved velocity field during the biflagellate's power stroke measured in a thin liquid film. The insets show instantaneous flagellar conformations. Figure modified from Guasto et al. (2010) with permission. Copyright 2010 by The American Physical Society. (*d*) Particle velocimetry measurements of the flow field generated by *Volvox carteri*, showing that the dominant contribution to the flow field comes from a Stokeslet, revealed that this colonial green alga is not force-free, an unexpected result in view of its small density contrast with water. Figure modified from Drescher et al. (2010a) with permission. Copyright 2010 by The American Physical Society. (*e*) When the Stokeslet contribution is removed, the flow field of *V. carteri* is dominated by the source dipole term. Figure modified from Drescher et al. (2010a) with permission. Copyright 2010 by The American Physical Society. Microorganisms are swimming to the right in panels *a–c* and vertically upward in panels *d* and *e*. Lines represent streamlines, and colors or arrows show the fluid velocity, with approximate maximum velocities of (*a*) 3.2, (*b*) 110, (*c*) 400, (*d*) 300, and (*e*) 150 μm s^{-1}.

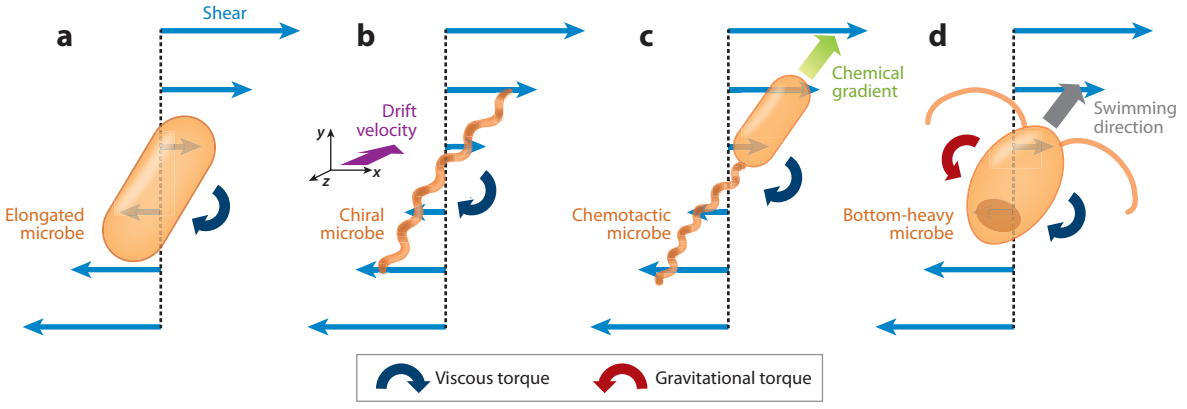

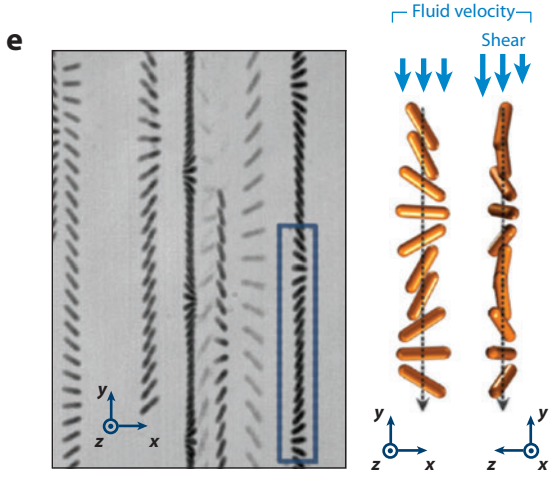

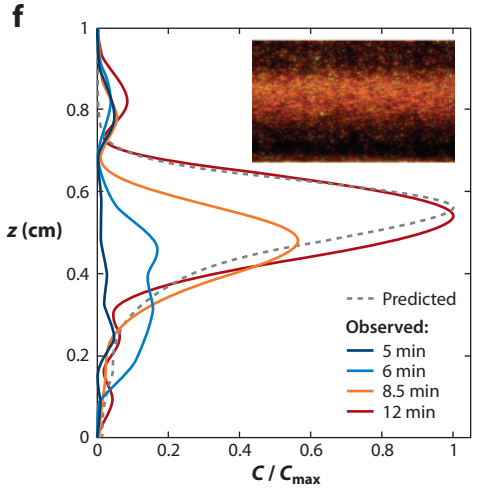

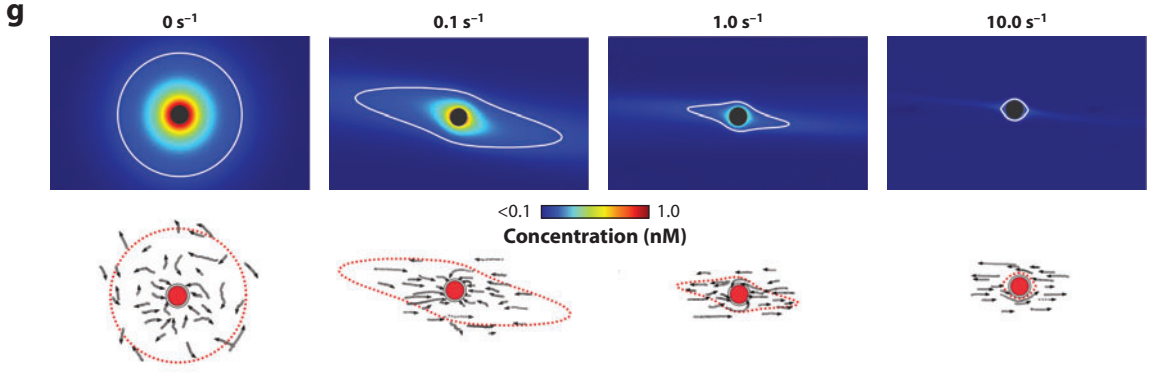

orbits (**Figure 3*e***; Kaya & Koser 2009), modified by the presence of the microchannel surfaces. Observations in steady shear showed a linear increase of the rotation period with aspect ratio for a rigid diatom chain, but not for a more flexible one (Karp-Boss & Jumars 1998). Both species had smaller periods than predicted for spheroids, in agreement with results for permanently bent particles (Forgacs & Mason 1959). Highly flexible chains could further coil and self-entangle (Forgacs & Mason 1959, Lindstrom & Uesaka 2007).

The rotation of phytoplankton in shear can affect light propagation in the upper ocean due to the dependence of scattering on cell orientation. Because a considerable fraction of the larger (>5 μm) phytoplankton are elongated (see Section 1 and **Figure 1*f*,*l***) and typical marine shear rates are predicted to be sufficient to align them (i.e., $Pe_r > 1$), the effect can be substantial and was estimated to increase backscattering by up to 35% (Marcos et al. 2011b).

Chirality introduces a twist on Jeffery orbits (**Figure 3*b*,*c***). Chirality abounds among microorganisms: Prokaryotic flagella are chiral, and spirochaetes have helically coiled bodies. For elongated chiral organisms, the coupling of Jeffery orbits with the shape asymmetry causes cells to drift across streamlines (Makino & Doi 2005). This chiral drift was recently observed for nonmotile bacteria (*Leptospira biflexa*) in a microchannel (Marcos et al. 2009).

3.2. Gyrotaxis

Several flagellates, protists, and larvae preferentially swim upward (Pedley & Kessler 1992, Pennington & Strathmann 1990, Roberts 1970). This phenomenon, called gravitaxis, has long been observed (Wager 1911), yet controversy remains as to the underlying mechanism: active sensing response or passive torque. Experiments in micro- and hypergravity suggested the presence of a gravity receptor in ciliates such as *Euglena* (Häder et al. 2003); internal vacuoles in *Loxodes* might act as gravity sensors, as do statocysts in aquatic invertebrates (Fenchel & Finlay 1984), whereas *Stylonychia mytilus* modulates the membrane potential in response to spatial orientation (Krause et al. 2010). However, the shape-induced drag asymmetry of ciliates such as *Paramecium* might also cause gravitaxis, as suggested by experiments with scale models

Figure 3

The effect of ambient flow on planktonic microorganisms. Shear can have multiple effects on microorganisms, including (*a*) elongated organisms, for which shear determines orbits and periods of rotation (Jeffery 1922); (*b*) chiral microbes, such as helically shaped bacteria (e.g., spirochetes), for which shear induces a drift across streamlines (Marcos et al. 2009) (a right-handed helical microbe drifts in the third dimension, into the page); (*c*) chemotactic microbes, for which shear hampers their attempt to navigate chemical gradients (Locsei & Pedley 2009b); and (*d*) gyrotactic microbes, whose swimming direction is determined by shear (Kessler 1985). (*e*) High-speed tracking of deflagellated *Escherichia coli* bacteria as they are transported by a shear flow near the surface of a microfluidic device (*left*) and reconstruction of the cells' periodic orbiting motion (*right*). Figure modified from Kaya & Koser (2009) with permission. Copyright 2009 by The American Physical Society. (*f*) Gyrotaxis in spatially variable shear can trap cells at specific depths, resulting in the formation of thin plankton layers, as shown here for *Chlamydomonas nivalis* (*line plot*) and *Heterosigma akashiwo* (*inset*). Vertical profiles represent observed distributions of cells (*solid lines*), acquired at different times (5 to 12 min) after the release of cells in the flow chamber, along with the prediction from a numerical model of gyrotaxis (*dashed line*). No layer was observed to form using dead cells. Figure modified from Durham et al. (2009) with permission. (*g*) In marine environments, many bottom-dwelling organisms such as mollusks and sea urchins reproduce by broadcasting gametes into the open ocean, where fertilization takes place (external fertilization). The chemoattractant plumes released by female gametes (eggs) are distorted by shear, which extends the range of the chemoattractant but also dilutes its concentration. Shown on the top row are the modeled attractant concentrations emitted by a 200-μm-diameter abalone egg in a linear shear, for the shear rates 0, 0.1, 1.0, and 10.0 s^{-1} (*left to right*). Shown on the bottom row are the observed sperm trajectories in the vicinity of eggs under the same conditions, illustrating that high shear rates hamper the sperms' ability to find the egg, likely due to a combination of the depleted chemical signal and the overpowering torque due to the shear. Alternatively, extension of the plume at small shear rates (0.1 s^{-1}) enhances the probability of fertilization. Figure modified from Zimmer & Riffell (2011) with permission.

(Jonsson et al. 1991, Roberts & Deacon 2002). Furthermore, passive torques due to posteriorly located heavy organelles (bottom-heaviness) reorient small flagellates such as *Chlamydomonas* (Kessler 1985).

Peritrichous: bacteria with multiple flagella emanating from all over the cell body

Monotrichous: bacteria with a single flagellum

In flow, the interaction between swimming, gravitational torque, and hydrodynamic torque results in directed locomotion, termed gyrotaxis (**Figure 3*d***) (Kessler 1985). Using Jeffery's theory (Equation 5), the orientation **p** of a spheroidal gyrotactic cell obeys

$$\dot{\mathbf{p}} = \frac{1}{2B}[\mathbf{k} - (\mathbf{k}\cdot\mathbf{p})\mathbf{p}] + \frac{1}{2}\boldsymbol{\omega}\times\mathbf{p} + \beta\mathbf{p}\cdot\mathbf{E}\cdot(\mathbf{I}-\mathbf{pp}), \quad (6)$$

where **k** is the unit upward vector, $B = \mu\alpha/(2g\rho h)$ a timescale for reorientation by gravity, ρ the mean cell density, g is the acceleration due to gravity, α a dimensionless resistance to rotation, and h the displacement of the center of mass (Brenner 1970; Pedley & Kessler 1987, 1992).

Equation 6 predicts a stable swimming direction relative to the vertical, θ, for shear rates $\dot{\gamma}$ below a critical value. For spherical cells in a simple shear flow, with the velocity gradient parallel to gravity, $\sin\theta = B\dot{\gamma}$ for $\dot{\gamma} < B^{-1}$ (the equilibrium regime), whereas for $\dot{\gamma} > B^{-1}$, the gravitational torque cannot compensate for the viscous spin, and cells tumble end over end (the tumbling regime). For spheroidal cells, the critical shear rate further depends on elongation, although the effective eccentricity is diminished by the beating of the flagella (O'Malley & Bees 2011). Variability among individuals shifts θ toward the vertical axis, and surprisingly, a stable swimming direction exists for all shear rates provided that viscous and gravitational torques are not aligned (Thorn & Bearon 2010).

Gyrotaxis can drive patchiness in phytoplankton distributions. The accumulation of *C. nivalis* in downwelling flow dates back to Kessler's (1985) first, elegant experiments on gyrotaxis. In spatially varying shear, gyrotaxis can trap cells at specific depths, where shear surpasses B^{-1}. This can result in the formation of thin phytoplankton layers, as observed for *C. nivalis* and the toxic *Heterosigma akashiwo* (**Figure 3*f***) (Durham et al. 2009). Strong cell accumulation could in turn induce Rayleigh-Bénard-type instabilities in a process called bioconvection (Pedley 2010), which is beyond the scope of this article.

3.3. Chemotaxis and Fertilization

Despite the ubiquitous presence of flow in aquatic environments, little is known about how flow affects motility, especially during chemotaxis. Peritrichous bacteria (**Figure 1*j***), such as *E. coli*, *Salmonella typhimurium*, and *Bacillus subtilis*, swim in the well-known run-and-tumble pattern (Berg & Brown 1972). Geometric and hydrodynamic interactions make flagella bundle together (Kim et al. 2004, Reichert & Stark 2005), forming a thick helix that propels the cell in a nearly straight run. After a short time, one or more motors reverse direction, the bundle comes undone, and the cell tumbles, reorienting by a nearly random angle θ ($\langle\theta\rangle = 68°$ for *E. coli*), before a new run begins. The tumble is a complex process during which polymorphic transformations temporarily alter the pitch and diameter of a flagellum (Turner et al. 2000). At long times, this mode of motility results in a random walk, with diffusivity comparable with that of small molecules (Berg 2004). By delaying tumbles when swimming up favorable chemical gradients, bacteria bias the walk, resulting in chemotaxis.

Monotrichous bacteria (**Figure 1*m***), prevalent in marine environments (Johansen et al. 2002), have been described as swimming in a run-and-reverse pattern (Mitchell et al. 1996), in which tumbles are replaced by ≈180° reversals of the swimming direction. However, this might be a hybrid run-and-flick pattern, recently reported for *Vibrio alginolyticus* and *Pseudoalteromonas haloplanktis* (Xie et al. 2011). In this strategy, the forward run is followed by a reversal to a backward

run, which in turn is succeeded by a flick, consisting of a sharp off-axis motion of the flagellum that causes a random reorientation of the cell ($\langle\theta\rangle \approx 90°$). The same two species also displayed rapid chemotaxis, markedly outperforming *E. coli* (Stocker et al. 2008, Xie et al. 2011), possibly because of faster chemosensory responses (Stocker 2011). The link between high-performance chemotaxis and flicks remains unknown.

An intriguing hypothesis is that reversers (i.e., run-and-reverse or run-and-flick swimmers) have an advantage for chemotaxis in flow (Stocker 2011). Models predict that a simple shear flow hampers chemotaxis in general, but less so for reversers compared with tumblers (Locsei & Pedley 2009b). Reversers can better retain their position near a nutrient source, such as a phytoplankter exuding organic solutes, markedly increasing uptake (Luchsinger et al. 1999). Reversers have been observed to accurately track swimming phytoplankton (Barbara & Mitchell 2003), although this could be a purely physical mechanism in which bacteria are suitably reoriented by shear in the phytoplankter's wake (Locsei & Pedley 2009a). Furthermore, no effect of reversals was predicted for chemotaxis in the wake of sinking particles (Kiørboe & Jackson 2001).

Shear also affects external fertilization. Many bottom-dwelling marine organisms, such as sea urchins and abalone, reproduce externally by broadcasting their gametes—sperm and eggs—into the ocean. Understanding fertilization rates is of great importance for demographics, fisheries, and ecosystem dynamics (Riffell & Zimmer 2007). The combination of physicochemical processes and the disparate length scales involved makes fertilization one of the most important, yet least understood natural processes. The rate-limiting step in broadcast spawning is the encounter of male and female gametes (proportional to the instantaneous local concentration of both) because the egg and sperm are released far from each other (>10 cm).

At low levels of turbulence, fertilization rates increase with turbulent intensity (Denny et al. 2002). This might result from a counterintuitive aspect of scalar transport in chaotic flows, in which distant parcels of gamete-containing fluid are stretched into concentrated filaments and folded into one another (Crimaldi & Browning 2004), enhancing long-range encounters between gametes. This process is not captured by a mean field approach, which predicts dilution by mixing, hence low fertilization. Conversely, fertilization rates plummet if turbulence is too intense (Denny et al. 2002), likely because at high shear rates [$>3\ s^{-1}$ for abalone (Riffell & Zimmer 2007)], sperm succumb to fluid torques, rotating in Jeffery orbits (see Section 3.1) that hamper progress toward the egg. At the scale of gametes, fertilization can be enhanced by chemotaxis (Riffell & Zimmer 2007, Ward et al. 1985). Eggs release attractants that sperm sense by swimming in helical trajectories (Crenshaw 1996). Flow further affects fertilization by deforming attractant plumes (**Figure 3*g***): At low shear rates, flow promotes fertilization by increasing the extent of the chemical signal, whereas high shear rates dilute chemoattractants below levels detectable by the sperm, decreasing fertilization success. For abalone, optimal shear rates are $O(0.1\ s^{-1})$ (Riffell & Zimmer 2007, Zimmer & Riffell 2011).

3.4. Mechanosensing

Some microorganisms perceive their world through mechanosensing, the ability to sense hydromechanical signals. Setae on copepod antennae are refined mechanoreceptors (**Figure 1*e***; Strickler & Bal 1973), whose deformation elicits neurophysiological responses for velocity differences as small as $20\ \mu m\ s^{-1}$ (Kiørboe et al. 2009, Visser 2001). Prey use mechanosensing themselves to determine when they are being drawn into a copepod's feeding current: Both ciliates and flagellates perform powerful escape jumps when shear rates exceed $\sim$1–10 s^{-1} (Jakobsen 2001, 2002). Protists sense hydromechanical signals via changes in their membrane's electrical potential (Naitoh & Eckert 1969).

Osmotroph: organism that takes up dissolved nutrients from its surroundings via osmosis

It remains unclear whether spermatozoa can sense shear. Observations of spermatozoa pointing upstream in Poiseuille flow [referred to as rheotaxis (Bretherton & Rothschild 1961)] suggested this capability (Bretherton & Rothschild 1961), but subsequent experiments showed that upstream swimming can result from the hydrodynamic attraction of swimming sperm to surfaces, combined with shear-induced rotation (Rothschild 1963, Roberts 1970, Winet et al. 1984).

Mechanosensing appears unlikely for bacteria. Upstream swimming of *E. coli* was found to be a passive process resulting again from wall attraction (Hill et al. 2007), and microfluidic experiments with four bacterial strains showed no behavioral response to shear (Marcos et al. 2011a). An exception might be the polar flagellum of *Vibrio parahaemolyticus* (**Figure 1*m***) and *Proteus mirabilis*, which, upon inhibition of its rotation by an increase in ambient viscosity, induces the formation of a second, lateral flagella system. The polar flagellum thus would act as a dynamometer (McCarter et al. 1988), although how the cell senses its flagellum's impaired rotation remains unclear.

4. FEEDING IN FLOW

The life of planktonic microorganisms is largely regulated by encounters (Kiørboe 2008). Bacterial hosts encounter viruses, osmotrophs must encounter nutrient molecules, and some phytoplankton need to encounter conspecifics for sexual reproduction. Here we address the transport of dissolved nutrients to cells, a fundamental process for a large fraction of planktonic microorganisms, which feed by osmosis. We discuss the effect of flow on solute uptake, summarizing earlier work (Karp-Boss et al. 1996) and focusing on recent developments and open questions.

The concentration C of a solute in a flow field $\mathbf{u}$ is governed by the advection-diffusion equation, which in dimensionless form reads

$$\frac{\mathrm{Pe}}{\mathrm{Sr}}\frac{\partial \tilde{C}}{\partial \tilde{t}} + \mathrm{Pe}\,\tilde{\mathbf{u}}\cdot\tilde{\nabla}\tilde{C} = \tilde{\nabla}^2\tilde{C}, \tag{7}$$

where $\tilde{C} = C/C_0$ is the dimensionless concentration, and C_0 is a characteristic concentration. The Péclet number $\mathrm{Pe} = UL/D$ is the ratio of the diffusion timescale to the advection timescale, where D is the solute's diffusivity. The uptake rate, $\mathcal{I}$, is obtained by solving for $C(\mathbf{x}, t)$, computing the flux $-D\nabla C$ at the cell surface, and integrating it over the surface area. This is most often done under steady conditions ($\partial C/\partial t = 0$). Hence uptake depends on the solute's diffusivity and the concentration gradients at the cell surface (in addition to the organism's ability to shuttle nutrient molecules across its cell membrane using enzymes).

In the absence of flow, the uptake rate of a perfectly absorbing, spherical organism of radius R is $\mathcal{I} = 4\pi RDC_0$, where C_0 is the far-field concentration. Uptake scales with the radius, not surface area, because the concentration gradient depends inversely on the radius. The cell shape has a modest effect on uptake, with prolate ellipsoids having marginally greater uptake than spheres of equal volume (Clift et al. 2005). Some bacteria appear to exploit this effect by becoming elongated in nutrient-deprived conditions (Steinberger et al. 2002).

Flow can increase nutrient uptake by sweeping fresh solute into the vicinity of the cell. The Sherwood number, Sh, quantifies uptake enhancement due to flow (analogous to the Nusselt number in heat transfer) and is defined as the ratio of uptake in the presence of flow to uptake due solely to diffusion. Hence $\mathrm{Sh} = 1$ for pure diffusion and $\mathrm{Sh} = -D\int \nabla C\cdot\mathbf{n}\,dA/4\pi RDC_0$ for a sphere. The increase in uptake due to flow results from a steepening of the gradient at the cell surface and is customarily expressed as a relation between Sh and Pe for a given flow and cell shape (e.g., see **Figure 4*a***). Below we discuss the effect of flow on uptake for three cases: uniform motion relative to the fluid, such as in swimming or sinking; shear flows; and turbulence.

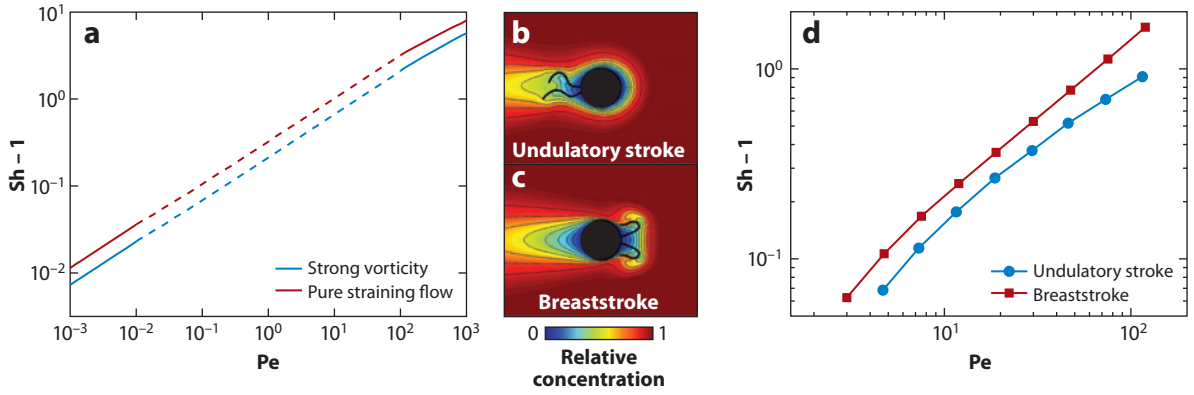

Figure 4

Nutrient uptake in flow. The departure of the Sherwood number, Sh, from 1 measures the increase in nutrient transport to a microorganism due to flow and is often expressed as a function of the Péclet number, Pe, which estimates the diffusion timescale relative to the advection timescale. The Sherwood number is analogous to the Nusselt number for heat transfer. (*a*) The dependence of the Sherwood number on the Péclet number for a spherical, osmotrophic microorganism in shear flow, for the case of pure straining flow (*red*) and of strong vorticity (*blue*). Vorticity reduces nutrient transport by causing streamlines to partially close around the organism, hampering exchange. The solid lines indicate theoretical solutions for $\mathrm{Pe}_{shear} \ll 1$ and $\mathrm{Pe}_{shear} \gg 1$, and dashed lines are the interpolated solutions, $\mathrm{Sh} = 1.004 + 0.32\mathrm{Pe}_{shear}^{1/2}$ (*red*) and $\mathrm{Sh} = 1.002 + 0.21\,\mathrm{Pe}_{shear}^{1/2}$ (*blue*) (Karp-Boss et al. 1996). Interpolation is made necessary by the dearth of information in the intermediate Péclet number regime. (*b*,*c*) A biflagellated osmotrophic swimmer can increase its uptake by beating its flagella to locally stir the concentration field. The images show how two commonly observed swimming gaits, the undulatory stroke (*b*) and the breaststroke (*c*), are predicted to change the local concentration field. Figure modified from Tam & Hosoi (2011a) with permission. (*d*) As a result of more effective local stirring of the fluid, the breaststroke, which is most commonly observed in nature, outperforms the undulatory stroke in terms of nutrient uptake. Here the Péclet number is defined on the basis of mechanical energy. Figure modified from Tam & Hosoi (2011a) with permission.

4.1. Sinking and Swimming

Significant attention has been devoted to understanding transport in a uniform flow past a fixed sphere, mostly at high Reynolds numbers (e.g., Kutateladze et al. 1982, and references therein). Whereas planktonic organisms are by definition untethered, this configuration is equivalent to a cell moving relative to a quiescent fluid under the action of an external force, as in gravitational settling. Because of our focus on microbes, we are concerned only with low–Reynolds number results. We include here the case of swimming, which has historically been considered analogous to settling (Karp-Boss et al. 1996). However, we discuss key differences stemming from the fact that force-free swimmers create a different flow field and thus a different concentration distribution compared with a settling organism (Bearon & Magar 2010, Magar et al. 2003, Tam & Hosoi 2011a).

The first quantitative treatment of the effect of fluid flow on nutrient uptake was applied to diatoms and dates back to Munk & Riley (1952). In the ensuing two decades, several fundamental relations were derived that apply to nutrient uptake. For a steadily moving sphere at $\mathrm{Re} \ll 1$, derivations based on asymptotic expansion yielded $\mathrm{Sh} = 1 + \mathrm{Pe}/2 + \mathrm{Pe}^2 \log(\mathrm{Pe})/2$ for $\mathrm{Pe} \ll 1$ (Acrivos & Taylor 1962) and $\mathrm{Sh} = 0.461 + 0.625\,\mathrm{Pe}^{1/3}$ for $\mathrm{Pe} \gg 1$ (Acrivos & Goddard 1965; see also Leal 2007). Clift et al. (2005) provided a fitting formula valid for all Péclet numbers: $\mathrm{Sh} = [1 + (1 + 2\,\mathrm{Pe})^{1/3}]/2$. Uptake increases by 22% at $\mathrm{Pe} = 1$ and doubles at $\mathrm{Pe} = 13$. For example, an $R = 1$-μm bacterium feeding on small organic molecules ($D = 10^{-9}$ m^2 s^{-1}) experiences an $\mathrm{Sh} - 1 = 0.5\%$–3% increase in uptake when swimming at typical speeds of 10–100 μm s^{-1}

(Pe = 0.01–0.1) compared with remaining stationary. Thus movement relative to the fluid has a negligible effect on the bacterial uptake of small nutrient molecules, such as nitrate or phosphate. Conversely, an $R = 100$-μm phytoplankter obtains an $\mathrm{Sh} - 1 = 62\%$–183% boost in uptake by swimming at typical speeds of 50–500 μm s^{-1}.

The relative magnitude of the advective enhancement depends intrinsically on the diffusivity. This is a simple yet important aspect to recognize in view of the wide molecular-weight range of dissolved organic matter in aquatic environments, with diffusivity spanning from $D = 10^{-12}$ to 10^{-9} m^2 s^{-1} (Amon & Benner 1994). The same $R = 1$-μm bacterium feeding on large molecules ($D = 10^{-12}$ m^2 s^{-1}) thus gains an $\mathrm{Sh} - 1 = 88\%$–243% increase in uptake from moving relative to the fluid.

In the above examples, we assume that swimming, which is force-free, is equivalent to sinking, or otherwise moving relative to the fluid under the action of an external force. As seen in Section 2, the flow fields associated with these two scenarios are fundamentally different, and these differences are expected to affect transport. Although we are not aware of a comprehensive treatment of this problem that systematically compares swimming and sinking in terms of the dependence of Sh on Pe, we summarize several recent findings that highlight the role of self-propulsion on uptake.

For a squirmer, an idealized ciliate that swims by generating a tangential surface velocity (see Section 2.3), models show an increase in mass transport scaling as $\mathrm{Sh} \sim \mathrm{Pe}^{1/2}$ (Magar et al. 2003). This is qualitatively different from the $\mathrm{Sh} \sim \mathrm{Pe}^{1/3}$ dependence (Acrivos & Goddard 1965) of a towed or sinking sphere and provides a clear illustration of the difference between sinking and swimming. How this dependence varies with organism morphology and propulsion kinematics remains to be studied.

That different flagellar beating patterns have different effects on transport, rather than just on propulsion, was recently shown for biflagellated phytoplankters such as *Chlamydomonas* (Tam & Hosoi 2011a). These authors calculated the optimal flagellar strokes for two fundamental biological functions, propulsion and nutrient uptake. They successfully predicted the two dominant gaits of *Chlamydomonas*, which switches between a breaststroke and an undulatory stroke (**Figure 4*b*,*c***). They showed that although both strokes optimize the swimming efficiency of the cell, the breaststroke outperforms the undulatory stroke in uptake efficiency because it causes larger distortions in the concentration field. Increases in nutrient uptake were as large as 25% for Pe = 7 (**Figure 4*d***), but no analytical relation between Sh and Pe was given.

Coordinated flagellar actions can also be used in a massively parallelized fashion by colonial microorganisms to increase their nutrient supply and relax the size limitation imposed by purely diffusive nutrient transport. The latter predicts a linearly increasing nutrient supply with increasing colony radius, yet metabolic cost increases with the colony's volume or, if cells are arranged on the colony's surface as in *Volvox*, with the square of the radius. In some organisms, such as the phytoplankter *Phaeocystis*, colony formation was observed to decrease the per-cell nutrient uptake, indicating that other selective pressures (e.g., reduced grazing rates associated with the larger size) are responsible for this colonial life-form (Ploug et al. 1999). *Volvox*, however, has been shown to use the coordinated flagellar motion of thousands of single, surface-mounted cells to stir the surrounding fluid. This increases the nutrient supply rate proportionally to the square of the radius, matching metabolic demand and circumventing the size bottleneck imposed by diffusive transport (Short et al. 2006, Solari et al. 2006).

4.2. Shear and Vorticity

Because nonmotile planktonic microorganisms are embedded in the flow, as their Stokes number (Ouellette et al. 2008) is very small, a uniform ambient flow does not influence uptake. The

lowest-order flow that affects uptake is then a linear variation in ambient flow velocity. This linear variation can take multiple forms, depending on the relative magnitude of the components of the rate of the strain tensor **E** and the vorticity tensor **Ω**. In particular, a spherical cell will rotate when there is vorticity, whereas it will not in a pure straining flow.

For an organism suspended in a linear velocity gradient of magnitude E, the appropriate Péclet number is based on the velocity difference ER across the length R of the organism, i.e., $\mathrm{Pe}_{shear} = R^2 E/D$. For $\mathrm{Pe}_{shear} \ll 1$, Batchelor (1979) derived the expression $\mathrm{Sh} = 1 + \alpha \mathrm{Pe}_{shear}^{1/2}$ (**Figure 4*a***), where $E = (E_{ij} E_{ij})^{1/2}$ (Frankel & Acrivos 1968) and α is within 10% of 0.34, depending on the particular flow, as long as vorticity is small compared to straining.

When the ambient vorticity is large, cell rotation partially suppresses the advective flux due to shear because streamlines wrap around the cell, and much of the same fluid recirculates without being refreshed. In this regime, Batchelor (1979) found $\mathrm{Sh} = 1 + 0.40\,\mathrm{Pe}_{shear*}^{1/2}$ (**Figure 4*a***), where $\mathrm{Pe}_{shear*} = R^2 E_\omega/D$, with $E_\omega = \omega \cdot \mathbf{E} \cdot \omega/\omega^2$ the shear rate in the direction parallel to the axis of rotation and ω the ambient vorticity (Batchelor 1979, Karp-Boss et al. 1996).

Asymptotic solutions have also been derived for $\mathrm{Pe}_{shear} \gg 1$, where $\mathrm{Sh} = \alpha \mathrm{Pe}_{shear}^{1/3}$ (**Figure 4*a***) with $0.9 \leq \alpha \leq 1.0$ for essentially all types of flow and α depending on the exact nature of the flow (Batchelor 1979), provided one defines $\mathrm{Pe}_{shear} = R^2 E_{rms}/D$ for pure straining flows (with E_{rms} the root mean square of the three principal components of **E**) and $\mathrm{Pe}_{shear} = \mathrm{Pe}_{shear*}$ for flows with vorticity.

The intermediate range ($0.01 < \mathrm{Pe}_{shear} < 100$) is not easily amenable to analytical solutions, yet it represents the regime experienced by many microorganisms. This can be seen by considering that $\mathrm{Pe} \approx 10^3\,\mathrm{Re}$ [as $\nu/D = O(10^3)$ for small molecules] and for many microorganisms $\mathrm{Re} = 10^{-5}$–10^{-1}. Although interpolations between small and large Péclet numbers are possible with comparatively little uncertainty (Batchelor 1979, Karp-Boss et al. 1996) (**Figure 4*a***), quantitative results are lacking and would be valuable in this regime.

Over 30 years ago, Batchelor (1979) called for experimental tests of the effect of velocity gradients on mass transport at low Reynolds numbers, yet observations have remained scarce to this day. Among the few experiments are those of Kutateladze et al. (1982), who verified that $\mathrm{Sh} \sim \mathrm{Pe}_{shear}^{1/3}$ for a sphere in a simple shear flow when $\mathrm{Pe}_{shear} \gg 1$ ($100 < \mathrm{Pe}_{shear} < 3,250$), using electrochemical measurements. Their observations fall within 10% of the prediction $\mathrm{Sh} = 0.9\mathrm{Pe}_{shear}^{1/3}$ (Batchelor 1979), despite the latter being valid for pure straining motion, whereas experiments were performed with a sphere held fixed in a flow with nonzero vorticity. More puzzling is Purcell's (1978) observation that the Sherwood number approaches $\mathrm{Sh} \sim \mathrm{Pe}^2$ for $\mathrm{Pe} < 1$, obtained by measuring the increase in heat exchange from a sphere kept at a constant temperature in a two-dimensional pure straining flow. The marked discrepancy in the exponent with the theoretical values of 1/2 to 1/3 likely stems from the presence of the container walls within four diameters from the sphere (Karp-Boss et al. 1996).

Experiments with organisms in both linear velocity gradients and turbulent flows (discussed in the following section) have largely proven inconclusive. Direct measurements of nutrient fluxes at the cellular scale are difficult; hence most experiments have relied on the quantification of uptake through growth rates. To complicate matters, uptake can depend on the physiological state and growth conditions of the cells, and experimental error can be large, yet even small differences in uptake can have a significant fitness advantage, as they will be compounded over many generations.

Measurements of leucine uptake by bacteria in a laminar shear flow did not reveal any increase in uptake (Logan & Kirchman 1991), as expected on the basis of the small size of bacteria; however, the large experimental error makes these experiments only a weak test of the theory. Pasciak & Gavis (1974) measured nitrate uptake by a ≈40-μm diatom in a Couette device, finding a maximum

increase in uptake of 10% for shear rates $\dot{\gamma} > 4\ s^{-1}$. For a shear rate of $\approx 0.5\ s^{-1}$, closer to typical marine values, the observed increase in uptake (2%) was an order of magnitude smaller than the one predicted for one-dimensional, steady shear flow ($Sh - 1 = 0.305\,Pe_{shear}^{1/2} = 24\%$) (Frankel & Acrivos 1968). Below we see that the opposite is true in turbulent flows, in which there is indication that flow effects on uptake are larger than predicted.

4.3. Turbulence

The majority of planktonic microorganisms are more minute than the smallest turbulent eddies, which measure ~10 Kolmogorov length scales [$\eta = (\nu^3/\epsilon)^{1/4}$] (Lazier & Mann 1989), or 10–30 mm for a turbulent dissipation rate $\epsilon = 10^{-6}$–$10^{-8}\ m^2\ s^{-3}$, typical of the upper mixed layer in the ocean (Gargett 1989). Consequently, microorganisms experience mostly linear spatial variations of fluid velocity. One can thus apply results from Section 4.2, by using $Pe_{turb} = R^2(\epsilon/\nu)^{1/2}/D$, where $(\epsilon/\nu)^{1/2}$ is the Kolmogorov-scale shear rate. This yields $Sh = 1 + 0.29\,Pe_{turb}^{1/2}$ for $Pe_{turb} \ll 1$ in isotropic turbulence (Karp-Boss et al. 1996) and $Sh = 0.55\,Pe_{turb}^{1/3}$ for $Pe_{turb} \gg 1$ and statistically steady turbulence (Batchelor 1980). For intermediate values ($0.01 < Pe_{turb} < 100$), Sh is bounded between $Sh = 1.014 + 0.15\,Pe_{turb}^{1/2}$ and $Sh = 0.955 + 0.344\,Pe_{turb}^{1/3}$ (Karp-Boss et al. 1996). These expressions, evaluated for typical dissipation rates, indicate that natural levels of turbulence affect only uptake by large microorganisms (≥60–100 μm) (Karp-Boss et al. 1996, Lazier & Mann 1989). For example, even a rather large, $R = 50$-μm cell absorbing small molecules under strong turbulence ($\epsilon = 10^{-6}\ m^2\ s^{-3}$) gains only a modest 18%–32% in nutrient uptake (Karp-Boss et al. 1996). Furthermore, the contribution of turbulence to enhanced uptake is typically weaker than the contributions from swimming or sinking (Lazier & Mann 1989).

Although experimental verifications of the theory exist for certain flows in the case of passive particles (Batchelor 1980), few are available for organisms. Observations of turbulence-enhanced uptake for the large ($R \approx 55$ μm) diatom *Coscinodiscus* sp. and the lack of enhancement for the small ($R \approx 6$ μm) *Thalassiosira pseudonana* are in agreement with theory (Peters et al. 2006). However, several reports of turbulence-induced growth increases for bacteria and phytoplankton remain difficult to reconcile with theory (Hondzo & Wüest 2009, Malits et al. 2004). In particular, Hondzo & Wüest (2009) measured a 1.8-fold growth increase for a ≈6-μm phytoplankton at $\epsilon = 3.5 \times 10^{-7}\ m^2\ s^{-3}$ and a 5.1-fold increase for *E. coli* at $\epsilon = 1.8 \times 10^{-4}\ m^2\ s^{-3}$. The explanation that Pe_{turb} should be based on the Kolmogorov velocity $(\epsilon\nu)^{1/4}$ rather than on $R(\epsilon/\nu)^{1/2}$ (Al-Homoud & Hondzo 2008) has no physical rationale, as uniform flow does not increase uptake. The cell aggregations observed in some of these studies also could not account for the increased uptake because their per-cell uptake is smaller than that of single cells, and the invoked bacterial turbulence structures occur only at very high cell concentrations (Dombrowski et al. 2004). This suggests that experimental artifacts, such as the temporary attachment of cells to surfaces or the leaching of high-molecular-weight compounds from decomposing cells, should be considered as possible culprits.

An important feature of turbulence is unsteadiness. Commonly occurring phytoplankton chains exposed to steady shear are predicted to have lower per-cell uptake than single cells (Pahlow et al. 1997). When the shear flow is oscillatory in time, with periods comparable with Kolmogorov timescales, diatom chains were predicted to have larger uptake than single cells in a two-dimensional model (Musielak et al. 2009). Because uptake peaks when an organism flips direction (Pahlow et al. 1997) (see the discussion of Jeffery orbits in Section 3.1), an increase in the rate of flipping due to unsteadiness might be responsible for the enhanced uptake

(P. Jumars, personal communication). Experiments to test these predictions would be highly valuable.

As chains grow longer and more flexible, deformation can affect nutrient uptake (Musielak et al. 2009). Although flexibility plays an insignificant role in uptake for uniform nutrient conditions, it reduces uptake by ≈10% compared with stiff chains in a patchy nutrient environment. Nutrients are often heterogeneously distributed in the ocean, where point sources such as phytoplankton lysis, excretions by larger organisms, and sinking marine particles release small [O (10–1,000 μm)] solute pulses. Flexible chains bend into compact conformations, which reduces their spatial extent and interactions with patches, suggesting a possible motivation for the evolution of rigid silica frustules on diatoms (Musielak et al. 2009).

Finally, turbulence can affect uptake by stirring nutrient patches. Chemotaxis allows microorganisms to exploit these patches (Blackburn 1998, Seymour et al. 2010, Stocker et al. 2008), yet fluid flow can interfere by stretching and folding patches and creating high-concentration filaments on the Batchelor scale, $\eta_B = (\nu D^2/\epsilon)^{1/4}$. For $\epsilon = 10^{-6}$–10^{-8} m^2 s^{-3}, $\eta_B = 30$–100 μm for small molecules ($D = 10^{-9}$ m^2 s^{-1}) and $\eta_B = 1$–3 μm for large molecules ($D = 10^{-12}$ m^2 s^{-1}). By affecting the nutrient gradients experienced by chemotactic organisms, turbulence can thus affect their uptake, as shown by recent simulations (Muñoz García et al. 2010, Taylor & Stocker 2011).

SUMMARY POINTS

1. The velocity field generated by a swimming microorganism is often approximated by simple far-field models, but only recently has it become possible to interrogate such flow fields directly. These observations have revealed that, although some swimmers are well described by simple far-field approximations, the flow field of others is overwhelmingly affected by small buoyancy contributions or exhibits a complex time dependence that is ill-described by current models.
2. Hydrodynamic shear can have multiple effects on microorganisms, from preferentially orienting elongated cells, to suppressing chemotaxis, to determining the swimming direction of gyrotactic plankton. These microhydrodynamic effects can have large-scale consequences, including the accumulation of cells at specific depths in the ocean and the regulation of light propagation in the water column by preferentially aligned phytoplankton.
3. Flow can enhance the uptake of dissolved nutrients, but not for the smallest organisms (≈1–10 μm), which live at low Péclet numbers, and rarely due to natural turbulence. Experimental measurements of the effects of flow on uptake are lagging significantly behind theoretical models, and current observations yield conflicting results.
4. The morphology and flagellar kinematics of several bacteria and phytoplankton species appear to be optimized for mechanical propulsion efficiency. However, for microorganisms that live at high Péclet numbers (∼1–1,000), the optimization of swimming must also take into account feeding, not just propulsion. Recent models have begun to link swimming kinematics with nutrient transport, but experimental confirmation is still lacking, and a comprehensive picture of the effects of swimming on uptake has not yet emerged.
5. Marine microorganisms provide a suite of specific adaptations, including fast chemotaxis, hybrid motility strategies, and high–Reynolds number jumps, which could provide fertile ground for the discovery of new biophysical mechanisms.

FUTURE ISSUES

1. Current mathematical models of self-propelled microorganisms require revision to account for recently observed discrepancies between real near-field flow fields and predicted far-field singularity solutions. How do these new findings affect the energetic cost of swimming, the interaction of cells with boundaries and each other, and the dynamics of dense suspensions?
2. How metabolically expensive microbial propulsion is remains unclear and is likely environment and species specific. Low propulsion costs entail a weak selective pressure on optimal morphologies and kinematics, yet models show that many microorganisms swim with optimally efficient flagellar appendages and beat strokes. How expensive is propulsion in the microbial world, and what are the ecological and evolutionary implications of swimming cost? Furthermore, how do microorganisms achieve the best compromise between optimal propulsion and optimal feeding?
3. The main function of microbial motility is to seek out nutrients and mates through the directional response to physical or chemical cues. Although models predict that shear strongly hampers tactic performance (e.g., chemotaxis), direct observation and a clear understanding of the ecological implications of the role of flow on motility and taxis are lacking.
4. Some microorganisms can sense and respond to fluid flow disturbances, but systematic and definitive experimental testing is needed to determine the underlying mechanism and how widespread this capability is across taxa (e.g., spermatozoa, bacteria).
5. Major breakthroughs would be the ability to directly measure uptake rates of microorganisms and to link measured single-cell flow fields with nutrient uptake enhancement. Furthermore, can we perform accurately controlled experiments on the effect of shear and turbulence on uptake?

DISCLOSURE STATEMENT

The authors are not aware of any biases that might be perceived as affecting the objectivity of this review.

ACKNOWLEDGMENTS

We thank Pete Jumars and Lee Karp-Boss for discussions on uptake in flow, William Durham for input on gyrotaxis, Tom Powers for discussions on microhydrodynamics, and Daniel Tam for information on optimal strokes of biflagellates. This work was supported by NSF grants OCE-0744641-CAREER and CBET-0966000 to R.S.

LITERATURE CITED

Acrivos A, Goddard J. 1965. Asymptotic expansions for laminar forced-convection heat and mass transfer. *J. Fluid Mech.* 23:273–91

Acrivos A, Taylor T. 1962. Heat and mass transfer from single spheres in Stokes flow. *Phys. Fluids* 5:387–94

Afanasyev YD. 2004. Wakes behind towed and self-propelled bodies: asymptotic theory. *Phys. Fluids* 16:3235–38

Al-Homoud A, Hondzo M. 2008. Enhanced uptake of dissolved oxygen and glucose by *Escherichia coli* in a turbulent flow. *Appl. Microbiol. Biotechnol.* 79:643–55

Amon R, Benner R. 1994. Rapid cycling of high-molecular-weight dissolved organic matter in the ocean. *Nature* 369:549–52

Ardekani AM, Stocker R. 2010. Stratlets: low Reynolds number point-force solutions in a stratified fluid. *Phys. Rev. Lett.* 105:084502

Azam F, Fenchel T, Field JG, Gray JS, Meyer-Reil LA, Thingstad F. 1983. The ecological role of water-column microbes in the sea. *Mar. Ecol. Prog. Ser.* 10:257–63

Barbara G, Mitchell J. 2003. Bacterial tracking of motile algae. *FEMS Microbiol. Ecol.* 44:79–87

Batchelor GK. 1979. Mass transfer from a particle suspended in fluid with a steady linear ambient velocity distribution. *J. Fluid Mech.* 95:369–400

Batchelor GK. 1980. Mass transfer from small particles suspended in turbulent fluid. *J. Fluid Mech.* 98:609–23

Bearon RN, Magar V. 2010. Simple models of the chemical field around swimming plankton. *J. Plankton Res.* 32:1599–608

Berg HC. 2004. E. coli *in Motion*. New York: Springer

Berg HC, Brown DA. 1972. Chemotaxis in *E. coli*. *Nature* 239:500–4

Blackburn N, Fenchel T, Mitchell J. 1998. Microscale nutrient patches in planktonic habitats shown by chemotactic bacteria. *Science* 282:2254–56

Blake JR. 1971. A spherical envelope approach to ciliary propulsion. *J. Fluid Mech.* 46:199–208

Böhmer M, Van Q, Weyand I, Hagen V, Beyermann M, et al. 2005. Ca^{2+} spikes in the flagellum control chemotactic behavior of sperm. *EMBO J.* 24:2741–52

Boyd CM, Gradmann D. 2002. Impacts of osmolytes on buoyancy of marine phytoplankton. *Mar. Biol.* 141:605–18

Brennen C, Winet H. 1977. Fluid mechanics of propulsion by cilia and flagella. *Annu. Rev. Fluid Mech.* 9:339–98

Brenner H. 1970. Rheology of a dilute suspension of dipolar spherical particles in an external field. *J. Colloid Interface Sci.* 32:141–58

Bretherton FP. 1962. The motion of rigid particles in a shear flow at low Reynolds number. *J. Fluid Mech.* 14:284–304

Bretherton FP, Rothschild. 1961. Rheotaxis of spermatozoa. *Proc. R. Soc. Lond. B* 153:490–502

Chattopadhyay S, Moldovan R, Yeung C, Wu XL. 2006. Swimming efficiency of bacterium *Escherichia coli*. *Proc. Natl. Acad. Sci. USA* 103:13712–17

Provides the first measurement of the propulsion efficiency of swimming bacteria, confirming theoretical predictions.

Chattopadhyay S, Wu XL. 2009. The effect of long-range hydrodynamic interaction on the swimming of a single bacterium. *Biophys. J.* 96:2023–28

Childress S. 1981. *Mechanics of Swimming and Flying*. Cambridge, UK: Cambridge Univ. Press

Chisholm S, Olson R, Zettler E, Goericke R, Waterbury J, Welschmeyer N. 1988. A novel free-living prochlorophyte abundant in the oceanic euphotic zone. *Nature* 334:340–43

Clavano WR, Boss E, Karp-Boss L. 2007. Inherent optical properties of non-spherical marine-like particles: from theory to observation. *Oceanogr. Mar. Biol.* 45:1–38

Clift R, Grace JR, Weber ME. 2005. *Bubbles, Drops, and Particles*. New York: Dover

Crenshaw HC. 1996. A new look at locomotion in microorganisms: rotating and translating. *Am. Zool.* 36:608–18

Crimaldi J, Browning H. 2004. A proposed mechanism for turbulent enhancement of broadcast spawning efficiency. *J. Mar. Syst.* 49:3–18

Denny MW, Nelson EK, Mead KS. 2002. Revised estimates of the effects of turbulence on fertilization in the purple sea urchin, *Strongylocentrotus purpuratus*. *Biol. Bull.* 203:275–77

Di Leonardo R, Dell'Arciprete D, Angelani L, Iebba V. 2011. Swimming with an image. *Phys. Rev. Lett.* 106: 038101

DiLuzio WR, Turner L, Mayer M, Garstecki P, Weibel DB, et al. 2005. *Escherichia coli* swim on the right-hand side. *Nature* 435:1271–74

Dombrowski C, Cisneros L, Chatkaew S, Goldstein RE, Kessler JO. 2004. Self-concentration and large-scale coherence in bacterial dynamics. *Phys. Rev. Lett.* 93:2–5

Drescher K, Dunkel J, Cisneros LH, Ganguly S, Goldstein RE. 2011. Fluid dynamics and noise in bacterial cell–cell and cell–surface scattering. *Proc. Natl. Acad. Sci. USA* 108:10940–45

Provides the first measurement of the flow field around free-swimming phytoplankton, demonstrating the limitations of classic singularity models.

Drescher K, Goldstein RE, Michel N, Polin M, Tuval I. 2010a. Direct measurement of the flow field around swimming microorganisms. *Phys. Rev. Lett.* 105:168101

Drescher K, Goldstein RE, Tuval I. 2010b. Fidelity of adaptive phototaxis. *Proc. Natl. Acad. Sci. USA* 107:11171–76

Drescher K, Leptos KC, Goldstein RE. 2009. How to track protists in three dimensions. *Rev. Sci. Instrum.* 80:014301

Durham WM, Kessler JO, Stocker R. 2009. Disruption of vertical motility by shear triggers formation of thin phytoplankton layers. *Science* 323:1067–70

Dusenbery D. 2009. *Living at Micro Scale: The Unexpected Physics of Being Small*. Cambridge, MA: Harvard Univ. Press

Engelmann TW. 1883. Bacterium photometricum. *Pflüg. Arch. Gesamte Physiol.* 30:95–124

Fenchel T, Finlay BJ. 1984. Geotaxis in the ciliated protozoan *Loxodes*. *J. Exp. Biol.* 110:17–33

Field C, Behrenfeld M, Randerson J, Falkowski P. 1998. Primary production of the biosphere: integrating terrestrial and oceanic components. *Science* 281:237–40

Forgacs OL, Mason SG. 1959. Particle motions in sheared suspensions X. Orbits of flexible threadlike particles. *J. Colloid Sci.* 14:473–91

Frankel N, Acrivos A. 1968. Heat and mass transfer from small spheres and cylinders freely suspended in shear flow. *Phys. Fluids* 11:1913–18

Frankel RB, Bazylinski DA, Johnson MS, Taylor BL. 1997. Magneto-aerotaxis in marine coccoid bacteria. *Biophys. J.* 73:994–1000

Gadêlha H, Gaffney EA, Smith DJ, Kirkman-Brown JC. 2010. Nonlinear instability in flagellar dynamics: a novel modulation mechanism in sperm migration? *J. R. Soc. Interface* 7:1689–97

Gaffney EA, Gadêlha H, Smith DJ, Blake JR, Kirkman-Brown JC. 2011. Mammalian sperm motility: observation and theory. *Annu. Rev. Fluid Mech.* 43:501–28

Gargett AE. 1989. Ocean turbulence. *Annu. Rev. Fluid Mech.* 21:419–51

Goldstein RE, Polin M, Tuval I. 2009. Noise and synchronization in pairs of beating eukaryotic flagella. *Phys. Rev. Lett.* 103:168103

Gray J, Hancock G. 1955. The propulsion of sea-urchin spermatozoa. *J. Exp. Biol.* 32:802–14

Guasto JS, Johnson KA, Gollub JP. 2010. Oscillatory flows induced by microorganisms swimming in two dimensions. *Phys. Rev. Lett.* 105:168102

Gueron S, Levit-Gurevich K. 1999. Energetic considerations of ciliary beating and the advantage of metachronal coordination. *Proc. Natl. Acad. Sci. USA* 96:12240–45

Gueron S, Levit-Gurevich K, Liron N, Blum J. 1997. Cilia internal mechanism and metachronal coordination as the result of hydrodynamical coupling. *Proc. Natl. Acad. Sci. USA* 94:6001–6

Guirao B, Joanny JF. 2007. Spontaneous creation of macroscopic flow and metachronal waves in an array of cilia. *Biophys. J.* 92:1900–17

Häder DP, Lebert M, Richter P, Ntefidou M. 2003. Gravitaxis and graviperception in flagellates. *Space Life Sci.* 31:2181–86

Hancock GJ. 1953. The self-propulsion of microscopic organisms through liquids. *Proc. R. Soc. Lond. A* 217:96–121

Hill J, Kalkanci O, McMurry JL, Koser H. 2007. Hydrodynamic surface interactions enable *Escherichia coli* to seek efficient routes to swim upstream. *Phys. Rev. Lett.* 98:068101

Hondzo M, Wüest A. 2009. Do microscopic organisms feel turbulent flows? *Environ. Sci. Technol.* 43:764–68

Ishijima S, Hamaguchi MS, Naruse M, Ishijima SA, Hamaguchi Y. 1992. Rotational movement of a spermatozoon around its long axis. *J. Exp. Biol.* 163:15–31

Jakobsen H. 2001. Escape response of planktonic protists to fluid mechanical signals. *Mar. Ecol. Prog. Ser.* 214:67–78

Jakobsen H. 2002. Escape of protists in predator-generated feeding currents. *Aquat. Microb. Ecol.* 26:271–81

Experimentally and mathematically demonstrated that gyrotaxis can have ecosystem-level consequences by concentrating marine phytoplankton into thin layers.

Provides the first demonstration of the unsteady nature of the flow field around a free-swimming phytoplankton throughout the beat cycle.

Jeffery GB. 1922. The motion of ellipsoidal particles immersed in a viscous fluid. *Proc. R. Soc. Lond. A* 102:161–79

Jenkinson IR. 1986. Oceanographic implications of non-Newtonian properties found in phytoplankton cultures. *Nature* 323:435–37

Jiang H. 2011. Why does the jumping ciliate *Mesodinium rubrum* possess an equatorially located propulsive ciliary belt? *J. Plankton Res.* 33:998–1011

Jiang H., Kiørboe T. 2011a. Propulsion efficiency and imposed flow fields of a copepod jump. *J. Exp. Biol.* 214:476–86

Jiang H, Kiørboe T. 2011b. The fluid dynamics of swimming by jumping in copepods. *J. R. Soc. Interface* 8:1090–103

Johansen J, Pinhassi J, Blackburn N, Zweifel U, Hagström A. 2002. Variability in motility characteristics among marine bacteria. *Aquat. Microb. Ecol.* 28:229–37

Johnson RE, Brokaw CJ. 1979. Flagellar hydrodynamics: a comparison between resistive-force theory and slender-body theory. *Biophys. J.* 25:113–27

Johnson ZI, Zinser ER, Coe A, McNulty NP, Woodward EMS, Chisholm SW. 2006. Niche partitioning among *Prochlorococcus* ecotypes along ocean-scale environmental gradients. *Science* 311:1737–40

Jonasz M. 1987. Nonsphericity of suspended marine particles and its influence on light scattering. *Limnol. Oceanogr.* 32:1059–65

Jonsson P, Andre C, Lindegarth M. 1991. Swimming behaviour of marine bivalve larvae in a flume boundary-layer flow: evidence for near-bottom confinement. *Mar. Ecol. Prog. Ser.* 79:67–76

Karp-Boss L, Boss E, Jumars P. 1996. Nutrient fluxes to planktonic osmotrophs in the presence of fluid motion. *Oceanogr. Mar. Biol.* 34:71–107

Karp-Boss L, Jumars P. 1998. Motion of diatom chains in steady shear flow. *Limnol. Oceanogr.* 43:1767–73

Kaya T, Koser H. 2009. Characterization of hydrodynamic surface interactions of *Escherichia coli* cell bodies in shear flow. *Phys. Rev. Lett.* 103:138103

Keller S, Wu T. 1977. A porous prolate-spheroidal model for ciliated micro-organisms. *J. Fluid Mech.* 80:259–78

Kessler J. 1985. Hydrodynamic focusing of motile algal cells. *Nature* 313:218–20

Kim MJ, Kim MJ, Bird JC, Park J, Powers TR, Breuer KS. 2004. Particle image velocimetry experiments on a macro-scale model for bacterial flagellar bundling. *Exp. Fluids* 37:782–88

Kiørboe T. 2008. *A Mechanistic Approach to Plankton Ecology*. Princeton, NJ: Princeton Univ. Press

Kiørboe T, Andersen A, Langlois VJ, Jakobsen HH, Bohr T. 2009. Mechanisms and feasibility of prey capture in ambush-feeding zooplankton. *Proc. Natl. Acad. Sci. USA* 106:12394–99

Kiørboe T, Jackson GA. 2001. Marine snow, organic solute plumes, and optimal chemosensory behavior of bacteria. *Limnol. Oceanogr.* 46:1309–18

Kirchman DL. 2008. *Microbial Ecology of the Oceans*. New York: Wiley

Koch DL, Subramanian G. 2011. Collective hydrodynamics of swimming microorganisms: living fluids. *Annu. Rev. Fluid Mech.* 43:637–59

Krause M, Bräucker R, Hemmersbach R. 2010. Gravikinesis in *Stylonychia mytilus* is based on membrane potential changes. *J. Exp. Biol.* 213:161–71

Kröger N, Poulsen N. 2008. Diatoms: from cell wall biogenesis to nanotechnology. *Annu. Rev. Genet.* 42:83–107

Kutateladze SS, Nakoryakov VE, Iskakov MS. 1982. Electrochemical measurements of mass transfer between a sphere and liquid in motion at high Péclet numbers. *J. Fluid Mech.* 125:453–62

Lauga E, Powers TR. 2009. The hydrodynamics of swimming microorganisms. *Rep. Prog. Phys.* 72:096601

Lazier J, Mann K. 1989. Turbulence and the diffusive layers around small organisms. *Deep-Sea Res. A* 36:1721–33

Leal LG. 2007. *Advanced Transport Phenomena*. Cambridge, UK: Cambridge Univ. Press

Li G, Tang J. 2009. Accumulation of microswimmers near a surface mediated by collision and rotational Brownian motion. *Phys. Rev. Lett.* 103:078101

Lighthill MJ. 1952. On the squirming motion of nearly spherical deformable bodies through liquids at very small Reynolds numbers. *Commun. Pure Appl. Math.* 5:109–18

Lighthill MJ. 1976. Flagellar hydrodynamics. *J. Soc. Ind. Appl. Math.* 18:161–230
Lindstrom SB, Uesaka T. 2007. Simulation of the motion of flexible fibers in viscous fluid flow. *Phys. Fluids* 19:113307
Locsei JT, Pedley TJ. 2009a. Bacterial tracking of motile algae assisted by algal cell's vorticity field. *Microb. Ecol.* 58:63–74
Locsei JT, Pedley TJ. 2009b. Run and tumble chemotaxis in a shear flow: the effect of temporal comparisons, persistence, rotational diffusion, and cell shape. *Bull. Math. Biol.* 71:1089–116

Predicted the effect of shear on chemotaxis for different motility strategies, showing that reversals are superior to tumbles in shear.

Logan BE, Kirchman DL. 1991. Uptake of dissolved organics by marine bacteria as a function of fluid motion. *Mar. Biol.* 111:175–81
Luchsinger R, Bergersen B, Mitchell J. 1999. Bacterial swimming strategies and turbulence. *Biophys. J.* 77:2377–86
Machin K. 1963. The control and synchronization of flagellar movement. *Proc. R. Soc. Lond. B* 158:88–104
Machin KE. 1958. Wave propagation along flagella. *J. Exp. Biol.* 35:796–806
Magar V, Goto T, Pedley TJ. 2003. Nutrient uptake by a self-propelled steady squirmer. *Q. J. Mech. Appl. Math.* 56:65–91
Makino M, Doi M. 2005. Migration of twisted ribbon-like particles in simple shear flow. *Phys. Fluids* 17:103605
Malits A, Peters F, Bayer-Giraldi M, Marrasé C, Zoppini A, et al. 2004. Effects of small-scale turbulence on bacteria: a matter of size. *Microb. Ecol.* 48:287–99
Marcos, Fu HC, Powers TR, Stocker R. 2009. Separation of microscale chiral objects by shear flow. *Phys. Rev. Lett.* 102:158103
Marcos, Fu HC, Powers TR, Stocker R. 2011a. Bacterial rheotaxis. Manuscript in review

Predicted that the coupling between the orientation distribution of plankton in shear and their light-scattering properties changes light propagation in the ocean.

Marcos, Seymour JR, Luhar M, Durham WM, Mitchell JG, et al. 2011b. Microbial alignment in flow changes ocean light climate. *Proc. Natl. Acad. Sci. USA* 108:3860–64
McCarter L, Hilmen M, Silverman M. 1988. Flagellar dynamometer controls swarmer cell differentiation of *V. parahaemolyticus*. *Cell* 54:345–51
Michelin S, Lauga E. 2010. Efficiency optimization and symmetry-breaking in a model of ciliary locomotion. *Phys. Fluids* 22:111901
Miklasz KA, Denny MW. 2010. Diatom sinking speeds: improved predictions and insight from a modified Stokes law. *Limnol. Oceanogr.* 55:2513–25
Mitchell JG, Pearson L, Dillon S. 1996. Clustering of marine bacteria in seawater enrichments. *Appl. Environ. Microbiol.* 62:3716–21
Mitchison TJ, Mitchison HM. 2010. How cilia beat. *Nature* 463:20–21
Moran MA, Buchan A, González JM, Heidelberg JF, Whitman WB, et al. 2004. Genome sequence of *Silicibacter pomeroyi* reveals adaptations to the marine environment. *Nature* 432:910–13
Munk W, Riley G. 1952. Absorption of nutrients by aquatic plants. *J. Mar. Res.* 11:215–40
Muñoz García J, Neufeld Z, Torney C. 2010. Nutrient exposure of chemotactic organisms in small-scale turbulent flows. *New J. Phys.* 12:103043
Musielak M, Karp-Boss L, Jumars P, Fauci L. 2009. Nutrient transport and acquisition by diatom chains in a moving fluid. *J. Fluid Mech.* 638:401–21
Naitoh Y, Eckert R. 1969. Ionic mechanisms controlling behavioral responses of *Paramecium* to mechanical stimulation. *Science* 164:963–65
Namba K, Vonderviszt F. 1997. Molecular architecture of bacterial flagellum. *Q. Rev. Biophys.* 30:1–65
Naselli-Flores L, Padisák J, Albay M. 2007. Shape and size in phytoplankton ecology: Do they matter? *Hydrobiologia* 578:157–61
O'Malley S, Bees MA. 2011. The orientation of swimming bi-flagellates in shear flows. *Bull. Math. Biol.* In press, doi:10.1007/s11538-011-9673-1
Ouellette NT, O'Malley PJJ, Gollub JP. 2008. Transport of finite-sized particles in chaotic flow. *Phys. Rev. Lett.* 101:174504
Padisák J, Soróczki-Pintér E, Rezner Z. 2003. Sinking properties of some phytoplankton shapes and the relation of form resistance to morphological diversity of plankton: an experimental study. *Hydrobiologia* 500:243–57
Pahlow M, Riebesell U, Wolf-Gladrow D. 1997. Impact of cell shape and chain formation on nutrient acquisition by marine diatoms. *Limnol. Oceanogr.* 42:1660–72

Pasciak W, Gavis J. 1974. Transport limitation of nutrient uptake in phytoplankton. *Limnol. Oceanogr.* 19:881–88

Paster E, Ryu WS. 2008. The thermal impulse response of *Escherichia coli*. *Proc. Natl. Acad. Sci. USA* 105:5373–77

Pedley TJ. 2010. Collective behaviour of swimming micro-organisms. *Exp. Mech.* 50:1293–301

Pedley TJ, Kessler JO. 1987. The orientation of spheroidal microorganisms swimming in a flow field. *Proc. R. Soc. Lond. B* 231:47–70

Pedley TJ, Kessler JO. 1992. Hydrodynamic phenomena in suspensions of swimming microorganisms. *Annu. Rev. Fluid Mech.* 24:313–58

Pennington JT, Strathmann RR. 1990. Consequences of the calcite skeletons of planktonic echinoderm larvae for orientation, swimming, and shape. *Biol. Bull.* 179:121–33

Peters F, Arin L, Marrase C, Berdalet E, Sala MM. 2006. Effects of small-scale turbulence on the growth of two diatoms of different size in a phosphorus-limited medium. *J. Mar. Syst.* 61:134–48

Pironneau O, Katz DF. 1974. Optimal swimming of flagellated micro-organisms. *J. Fluid Mech.* 66:391–415

Pizay MD, Lemee R, Simon N, Cras AL, Laugier JP, Dolan JR. 2009. Night and day morphologies in a planktonic dinoflagellate. *Protist* 160:565–75

Ploug H, Stolte W, Jørgensen BB. 1999. Diffusive boundary layers of the colony-forming plankton alga *Phaeocystis* sp.: implications for nutrient uptake and cellular growth. *Limnol. Oceanogr.* 44:1959–67

Polin M, Tuval I, Drescher K, Gollub JP, Goldstein RE. 2009. *Chlamydomonas* swims with two gears in a eukaryotic version of run-and-tumble locomotion. *Science* 325:487–90

Pomeroy LR. 1974. The ocean's food web, a changing paradigm. *BioScience* 24:499–504

Purcell EM. 1977. Life at low Reynolds number. *Am. J. Phys.* 45:3–11

Purcell EM. 1978. Effect of fluid motions on absorption of molecules by suspended particles. *J. Fluid Mech.* 84:551–59

Reichert M, Stark H. 2005. Synchronization of rotating helices by hydrodynamic interactions. *Eur. Phys. J. E* 17:493–500

Riffell JA, Zimmer RK. 2007. Sex and flow: the consequences of fluid shear for sperm-egg interactions. *J. Exp. Biol.* 210:3644–60

Rikmenspoel R. 1978. Movement of sea urchin sperm flagella. *J. Cell Biol.* 76:310–22

Roberts AM. 1970. Motion of spermatozoa in fluid streams. *Nature* 228:375–76

Roberts AM, Deacon FM. 2002. Gravitaxis in motile micro-organisms: the role of fore-aft body asymmetry. *J. Fluid Mech.* 452:405–23

Rothschild. 1963. Non-random distribution of bull spermatozoa in a drop of sperm suspension. *Nature* 198:1221–22

Rüffer U, Nultsch W. 1985. High-speed cinematographic analysis of the movement of *Chlamydomonas*. *Cell Motil. Cytoskel.* 5:251–63

Sartoris FJ, Thomas DN, Cornils A, Schnack-Schiel SB. 2010. Buoyancy and diapause in Antarctic copepods: the role of ammonium accumulation. *Limnol. Oceanogr.* 55:1860–64

Seymour JR, Simo R, Ahmed T, Stocker R. 2010. Chemoattraction to dimethylsulfoniopropionate throughout the marine microbial food web. *Science* 329:342–45

Short MB, Solari CA, Ganguly S, Powers TR, Kessler JO, Goldstein RE. 2006. Flows driven by flagella of multicellular organisms enhance long-range molecular transport. *Proc. Natl. Acad. Sci. USA* 103:8315–19

Solari CA, Ganguly S, Kessler JO, Michod RE, Goldstein RE. 2006. Multicellularity and the functional interdependence of motility and molecular transport. *Proc. Natl. Acad. Sci. USA* 103:1353–58

Spagnolie S, Lauga E. 2011. Comparative hydrodynamics of bacterial polymorphism. *Phys. Rev. Lett.* 106:058103

Steinberger RE, Allen AR, Hansma HG, Holden PA. 2002. Elongation correlates with nutrient deprivation in *Pseudomonas aeruginosa*–unsaturated biofilms. *Microb. Ecol.* 43:416–23

Stocker R. 2011. Reverse and flick: hybrid locomotion in bacteria. *Proc. Natl. Acad. Sci. USA* 108:2635–36

Stocker R, Seymour JR, Samadani A, Hunt DE, Polz MF. 2008. Rapid chemotactic response enables marine bacteria to exploit ephemeral microscale nutrient patches. *Proc. Natl. Acad. Sci. USA* 105:4209–14

Experimentally demonstrated that stirring caused by coordinated ciliary beating enhances *Volvox*'s nutrient uptake, overcoming a metabolic bottleneck for growth.

Computationally showed that the flagellar conformation typical of swimming bacteria (normal form) optimizes propulsion among all known polymorphisms.

Stone HA, Samuel AD. 1996. Propulsion of microorganisms by surface distortions. *Phys. Rev. Lett.* 77:4102–4

Strickler JR, Bal AK. 1973. Setae of the first antennae of the copepod *Cyclops scutifer* (Sars): their structure and importance. *Proc. Natl. Acad. Sci. USA* 70:2656–59

Mathematically demonstrated that common flagellar waveforms of biflagellates optimize swimming efficiency and, for the case of the breaststroke, nutrient uptake.

Tam D, Hosoi AE. 2011a. Optimal feeding and swimming gaits of biflagellated organisms. *Proc. Natl. Acad. Sci. USA* 108:1001–6

Tam D, Hosoi AE. 2011b. Optimal kinematics and morphologies for spermatozoa. *Phys. Rev. E* 83:045303

Taylor BL, Zhulin IB, Johnson MS. 1999. Aerotaxis and other energy-sensing behavior in bacteria. *Annu. Rev. Microbiol.* 53:103–28

Taylor G. 1951. Analysis of the swimming of microscopic organisms. *Proc. R. Soc. Lond. A* 209:447–61

Taylor JR, Stocker R. 2011. Trade-offs of chemotactic foraging in turbulent waters. Manuscript in preparation

Thorn GJ, Bearon RN. 2010. Transport of spherical gyrotactic organisms in general three-dimensional flow fields. *Phys. Fluids* 22:041902

Trevelyan B, Mason S. 1951. Particle motions in sheared suspensions. I. Rotations. *J. Colloid Sci.* 6:354–67

Turner L, Ryu WS, Berg HC. 2000. Real-time imaging of fluorescent flagellar filaments. *J. Bacteriol.* 182:2793–801

Villareal TA, Carpenter EJ. 2003. Buoyancy regulation and the potential for vertical migration in the oceanic cyanobacterium *Trichodesmium*. *Microb. Ecol.* 45:1–10

Visser AW. 2001. Hydromechanical signals in the plankton. *Mar. Ecol. Prog. Ser.* 222:1–24

Visser AW, Jonsson PR. 2000. On the reorientation of non-spherical prey particles in a feeding. *J. Plankton Res.* 22:761–77

Wager H. 1911. On the effect of gravity upon the movements and aggregation of *Euglena viridis*, Ehrb., and other micro-organisms. *Philos. Trans. R. Soc. Lond. B* 201:333–90

Walsby AE. 1994. Gas vesicles. *Microbiol. Rev.* 58:94–144

Walsby AE, Xypolyta A. 1977. Form resistance of chitan fibers attached to cells of *Thalassiosira fluviatilis* Hustedt. *Br. Phycol. J.* 12:215–23

Ward GE, Brokaw CJ, Garbers DL, Vacquier VD. 1985. Chemotaxis of *Arbacia punctulata* spermatozoa to resact, a peptide from the egg jelly layer. *J. Cell Biol.* 101:2324–29

Winet H, Bernstein GS, Head J. 1984. Obervations on the response of human spermatozoa to gravity, boundaries and fluid shear. *J. Reprod. Fertil.* 70:511–23

Woolley DM, Vernon GG. 2001. A study of helical and planar waves on sea urchin sperm flagella, with a theory of how they are generated. *J. Exp. Biol.* 204:1333–45

Wu TY. 1977. Hydrodynamics of swimming at low Reynolds numbers. *Fortschr. Zool.* 24:149–69

Observed a new, hybrid motility pattern of some monotrichous marine bacteria, a new compelling model system for locomotion.

Xie L, Altindal T, Chattopadhyay S, Wu X. 2011. Bacterial flagellum as a propeller and as a rudder for efficient chemotaxis. *Proc. Natl. Acad. Sci. USA* 108:2246–51

Young KD. 2006. The selective value of bacterial shape. *Microbiol. Mol. Biol. Rev.* 70:660–703

Zimmer RK, Riffell JA. 2011. Sperm chemotaxis, fluid shear, and the evolution of sexual reproduction. *Proc. Natl. Acad. Sci. USA* 108:13200–5

Zirbel M, Veron F, Latz M. 2000. The reversible effect of flow on the morphology of *Ceratocorys horrida* (Peridiniales, Dinophyta). *J. Phycol.* 36:46–58

RELATED RESOURCES

Berg HC. 1983. *Random Walks in Biology*. Princeton, NJ: Princeton Univ. Press

Denny M, Gaylord B. 2010. Marine ecomechanics. *Annu. Rev. Mar. Sci.* 2:89–114

Kim S, Karrila SJ. 2005. *Microhydrodynamics: Principles and Selected Applications*. New York: Dover

Annual Review of
Fluid Mechanics

Volume 44, 2012

Contents

Indexes

Errata

An online log of corrections to *Annual Review of Fluid Mechanics* articles may be found at http://fluid.annualreviews.org/errata.shtml